MARTIN MARIETTA ENERGY SYSTEMS LIBRARIES
3 4456 0361259 8

CENTRAL RESEARCH LIBRARY
DOCUMENT COLLECTION

cy. 4

ORNL-2521
Physics and Mathematics

cy. 4

MEASUREMENT OF ELECTRON FLUX IN MEDIA BOMBARDED BY X-RAYS

D. R. Nelson
R. D. Birkhoff
R. H. Ritchie
H. H. Hubbell, Jr.

CENTRAL RESEARCH LIBRARY
DOCUMENT COLLECTION
LIBRARY LOAN COPY
DO NOT TRANSFER TO ANOTHER PERSON
If you wish someone else to see this document, send in name with document and the library will arrange a loan.

OAK RIDGE NATIONAL LABORATORY
operated by
UNION CARBIDE CORPORATION
for the
U.S. ATOMIC ENERGY COMMISSION

LEGAL NOTICE

This report was prepared as an account of Government sponsored work. Neither the United States, nor the Commission, nor any person acting on behalf of the Commission:

A. Makes any warranty or representation, express or implied, with respect to the accuracy, completeness, or usefulness of the information contained in this report, or that the use of any information, apparatus, method, or process disclosed in this report may not infringe privately owned rights; or

B. Assumes any liabilities with respect to the use of, or for damages resulting from the use of any information, apparatus, method, or process disclosed in this report.

As used in the above, "person acting on behalf of the Commission" includes any employee or contractor of the Commission to the extent that such employee or contractor prepares, handles or distributes, or provides access to, any information pursuant to his employment or contract with the Commission.

ORNL-2521

Contract No. W-7405-eng-26

HEALTH PHYSICS DIVISION

MEASUREMENT OF ELECTRON FLUX IN MEDIA BOMBARDED BY X-RAYS

D. R. Nelson
R. D. Birkhoff
R. H. Ritchie
H. H. Hubbell, Jr.

Submitted as a thesis to the Faculty of the Graduate School of Vanderbilt University in partial fulfillment of the requirements for the degree of Master of Science in physics.

DATE ISSUED

OCT 13 1958

OAK RIDGE NATIONAL LABORATORY
Oak Ridge, Tennessee
operated by
UNION CARBIDE CORPORATION
for the
U. S. ATOMIC ENERGY COMMISSION

MARTIN MARIETTA ENERGY SYSTEMS LIBRARIES

3 4456 0361259 8

ACKNOWLEDGMENTS

I would like to express my sincere gratitude and appreciation to Drs. R. D. Birkhoff and H. H. Hubbell, Jr., (ORNL) for suggesting and supervising this thesis. I am deeply indebted to Dr. R. H. Ritchie, (ORNL), for his help with many of the theoretical calculations. I would also like to extend my appreciation to Mr. L. B. Farabee, (ORNL) and Dr. J. V. Cathcart, (ORNL), for their suggestions and aid in obtaining oxide-free copper spectrometer plates. Thanks are also due Mr. Hal Holzer, (ORNL), for his help with electronic troubles and to 1st. Lt. John C. Villforth, (USAF) for his assistance in taking data.

I would like to extend my appreciation to Dr. E. E. Anderson, (ORNL), and to the Oak Ridge Institute of Nuclear Studies which made possible my study at Vanderbilt University and this thesis work under an AEC Radiological Fellowship.

TABLE OF CONTENTS

	Page
Acknowledgments	ii
List of Tables	iv
List of Figures	v
I. Introduction	1
II. Theory	
A. Generation of Secondary Electrons in Media	6
B. Parallel Plate Spectrometer	7
C. I vs V for Assumed Energy Distribution	20
D. Energy Spectrum in Medium	22
E. The Saturation Current as a Function of the Parameters α and β	28
III. Apparatus	
A. X-Ray Machine	31
B. Parallel Plate Chambers	35
C. Electrical System	41
D. Vacuum System	45
IV. Experimental Procedure and Data Analysis	46
V. Experimental Results	50
VI. Conclusions	84
Appendix	
I. Sample Energy Distribution Calculation	86
II. A. Error Analysis	92
B. Sample Error Calculation for Annealed Copper	93
III. Summary of Abbreviations and Symbols	98
Bibliography	99

LIST OF TABLES

		Page
I.	Calculations of Chamber Plate Thickness	37
II.	Experimental Current Densities	56
III.	Energy Distribution in Copper (Hydrogen Annealed Surface)	77
IV.	Energy Distribution in Aluminum	78
V.	Energy Distribution in Graphite	79
VI.	Sample of Data and Analysis for Annealed Copper	87
VII.	Fermi Energy and Photoelectric Work Function for Cu, Al, and Graphite	90
VIII.	Error Analysis for Annealed Copper	94

LIST OF FIGURES

		Page
1.	Parallel Plate Spectrometer Cross Section	32
2.	Photograph of Parallel Plate Spectrometer	33
3.	Photograph of X-Ray Head and Vacuum System Enclosure	34
4.	Schematic Diagram of Apparatus	36
5.	Circuit of the Model Q-826-B Electrometer	42
6.	Circuit Schematic	43
7.	Straight Ahead, Isotropic and Cosine Emission Current-Voltage Curves Assuming Greening's Energy Distribution	51
8.	Current-Voltage Curves for Annealed Copper and for Greening's Isotropic Distribution	52
9.	Current-Voltage Curves for Aluminum and Greening's Isotropic Distribution	53
10.	Current-Voltage Curves for Graphite and Greening's Isotropic Distribution	54
11.	Comparison of Current-Voltage Curves for Three Copper Surfaces	57
12.	Current-Voltage Curve for Chemically Cleaned Copper	59
13.	Low Voltage Portion of Current-Voltage Curve for Chemically Cleaned Copper	60
14.	First Derivative of Current-Voltage Curve for Chemically Cleaned Copper	61
15.	Second Derivative of Current-Voltage Curve for Chemically Cleaned Copper	62
16.	Current-Voltage Curve for Annealed Copper	63

LIST OF FIGURES (Con't.)

		Page
17.	First Derivative of Current-Voltage Curve for Annealed Copper	64
18.	Second Derivative of Current-Voltage Curve for Annealed Copper	65
19.	Current-Voltage Curve for Aluminum	66
20.	First Derivative of Current-Voltage Curve for Aluminum	67
21.	Second Derivative of Current-Voltage Curve for Aluminum	68
22.	Current-Voltage Curve for Graphite	69
23.	First Derivative of Current-Voltage Curve for Graphite	70
24.	Second Derivative of Current-Voltage Curve for Graphite	71
25.	Energy Distribution for Chemically Cleaned Copper	73
26.	Energy Distribution for Annealed Copper	74
27.	Energy Distribution for Aluminum	75
28.	Energy Distribution for Graphite	76
29.	The Fit of the Function $\alpha/(\beta+E_w+V)^2$ to the Energy Distribution for Chemically Cleaned Copper	80
30.	The Fit of the Function $\alpha/(\beta+E_w+V)^2$ to the Energy Distribution for Annealed Copper	81
31.	The Fit of the Function $\alpha/(\beta+E_w+V)^2$ to the Energy Distribution for Aluminum	82
32.	The Fit of the Function $\alpha/(\beta+\phi+V)^2$ to the Energy Distribution for Graphite	83

ABSTRACT

The energy distribution of the electron flux generated by lightly filtered 250 KVCP X-rays has been determined for media consisting of pairs of parallel plates made of copper, aluminum or graphite. The space between the plates was kept at high vacuum and the plate current was recorded as a function of plate voltage. Saturation currents of .0063, .0011 and .00024 $\frac{esu}{cm^2 r}$ for the three chambers respectively were obtained at about 30 volts plate potential. All curves reached saturation at much lower applied voltages than would be expected from the energy distribution suggested by Greening. It was found possible to obtain the energy distributions from the first and second derivatives of the current-voltage curves. All distributions were fitted well with the function

$$\frac{\alpha}{\left[E - (E_W - 1)\right]^2} \quad \frac{esu}{cm^2 r \text{ volt}}$$

where E is the electron energy and E_W is the sum of the Fermi energy and the photoelectric work function, all in volts. The empirical constants α were found to be .11, .023 and .0021 $\frac{esu \text{ volts}}{cm^2 r}$ for the three media respectively where the E_W were taken to be 11.5, 15.9 and 4.6 volts.

I. INTRODUCTION

The basic unit of radiation exposure is the roentgen, which is defined in terms of the number of ion pairs or electrons formed per cubic centimeter of air, at standard temperature and pressure, by the passage of X or gamma radiation. Other units of radiation exposure such as the rep and rad are defined in terms of the amount of energy imparted to matter per unit of mass, in such a way that they represent about the same amount of energy deposition as the roentgen. Thus, the basic measurement of radiation exposure is still based upon the number of electrons or ions liberated in the medium by the passage of ionizing radiation.

However, experiments on biological systems indicate that biological damage depends not only upon the energy absorbed per unit mass, but also upon the type of the radiation (X, γ, β, α, neutrons, etc.) which produces the exposure. In fact, the difference in biological damage found for the same energy deposition from the different radiations has led to the introduction of a factor called the Relative Biological Effectiveness, which is characteristic of each radiation. The Relative Biological Effectiveness factor takes into account observed differences in biological damage, and provides a means for estimating biological damage by the physical measurement of ionization.

The importance of studying the spectra of low energy electrons in irradiated media or as an aid to understanding radiation damage has been pointed out by Platzman.[1] The present work has been directed at the measurement of the electron energy distribution in irradiated media in an effort to obtain some preliminary estimates of the distribution.

A related, but not identical problem has received considerable experimental attention in recent years. In this work, the energy spectrum of electrons ejected from surfaces by the action of corpuscular radiation has been measured. Wolff[2] has developed a theory of the electron energy distributions found for surfaces bombarded by electron beams and obtained approximate agreement with experiments.

Greening[3] has made a semi-quantitative estimate of the low energy electron distribution emerging from the walls of an irradiated chamber. Greening's low energy electron distribution is based on secondary emission experiments, and gives only 3% of the total number with energy in excess of 100 ev. In this distribution the number of electrons per unit energy interval for energies between 0 and 41 ev is given by $kve^{-V/8}$ and for energies greater than 41 ev is given by $64\ k/V^2$ where V is in ev.

---

1 Platzman, R. L., Rad. Res., 2, No. 1, 1 (1955).

2 Wolff, P. A., Phys. Rev. 95, No. 1, 56 (1954).

3 Greening, J. R., Brit. J. of Rad., 27, No. 315, 163 (1954).

Interpretation of secondary emission experiments is complicated by the boundary which is arbitrarily placed in the irradiated medium. Ideally, the medium should be of effectively infinite extent and bombarded isotropically in order to facilitate theoretical interpretation and to correspond more closely to radiation exposures found in biological systems. Experiments of this type have been carried out by Taylor[4] who has investigated the small currents which persist in irradiated ionization chambers even when the chambers are evacuated to a negligible pressure. Analysis to determine energy distribution of the electrons was complicated in his work by the use of a cylindrical chamber. Experiments similar to Taylor's are described in the present work, utilizing a parallel plate chamber, which is more readily amenable to theoretical analysis.

In the present work, the current-voltage curve for an evacuated parallel plate chamber is subject to simple theoretical interpretation such that the energy distribution of the secondary electrons may be obtained from it. However, it is necessary in the analysis to know the angular distribution for the secondary electrons emerging from the walls of the chamber in order to obtain their energy distribution. Whereas plausible arguments may be made for three such

---

[4] Taylor, L. S., Brit. J. of Rad., 24, No. 278, 67 (1951).

distributions, namely, the straight ahead, isotropic, and cosine, the resultant energy distribution obtained in these three cases depends strongly upon which of these is assumed. In order to avoid making any such assumption, it was found possible to calculate in the case of metals the angular distribution outside the surface using a classical picture of the barrier penetration, provided that the angular distribution inside the metal could be assumed to be isotropic. A calculation of this type yields the electron flux distribution inside the metal from the current-voltage curve.

McKay[5] in his review article on secondary emission has mentioned some of the many experimental difficulties found in the application of conventional electron spectrometers to low energy spectral measurements. The method used in this work avoids many of these problems. Since the path lengths in the parallel plate chamber are relatively short, a larger residual magnetic field may be tolerated without any large error being introduced. Also, the energy resolution of the chamber method is not limited by geometrical considerations but only by the accuracy with which chamber voltages and currents can be measured. Furthermore, the

---

[5] McKay, K. G., Advances in Electronics, 1, 65 (1948).

distortion of the energy distribution by the passage through the surface barrier may be more readily evaluated in the evacuated chamber experiments than in the secondary emission experiments because the flux in the medium is more nearly isotropic in the former than in the latter situation.

In the present work, X-rays of 250 kev maximum energy were directed at the chamber plates, producing Compton and photo-electrons, which in turn generated secondary electrons. The plates were made from copper, aluminum and graphite, and had a thickness approximately equal to the range of 250 kev electrons. Current-voltage measurements were made with potentiometers to insure data of sufficient accuracy to permit the extraction of first and second derivatives from these curves as required by the theoretical analysis. The electron energy distributions were then determined, and fitted with simple analytic functions. The saturation current is compared with that found by Taylor.

II. THEORY

A. Generation of Secondary Electrons in Media

Theories on the generation of secondary electrons in a medium have been given by Spencer and Fano[6] and by Wolff.[7] The Spencer-Fano treatment has been shown[8] to be approximately correct for electron energies above 30 kev and for a medium of low atomic number. Its validity below this energy has not been established. The essential ingredients of the Spencer-Fano theory are the Möller electron-electron cross section and the Bethe stopping power formula. Both of these have been accurately checked at energies above 100 kev, but await experimental verification below this energy. A more serious objection to the use of the Spencer-Fano theory at the low energies found here may be seen to arise from the consideration that the flux of electrons at energies of the order of the K shell binding energy and below depends upon atomic ionization cross sections and the stopping power corrected for shell effects. Thus it is probable that rather extensive modifications to the theory will be necessary before it may be expected to be valid at energies of a few electron volts.

Wolff has obtained a theoretical estimate of the electron flux in metals in the low energy region by solving the slowing

---

6 Spencer, L. V., and Fano, U., Phys. Rev., 93, 1172 (1954).

7 Wolff, op. cit.

8 Birkhoff, R. D., Hubbell, H. H. Jr., Cheka, J. S., and Ritchie, R. H., Health Physics Journal, 1, 27 (1958).

down equation using an electron-electron scattering cross section which is spherically symmetric in the center of mass system and is modified strongly by the exclusion principle operating in the conduction band. Wolff's results, strictly speaking, are only applicable to those electrons whose energy before scattering exceeds twice the Fermi energy in the metal. Most of the electrons measured in this work had energies less than twice the Fermi energy, and thus the theory is not applicable here. Furthermore, use of the spherically symmetric cross section is not valid for primary energies as high as those employed here (250 kev).

B. Parallel Plate Spectrometer

In considering the relationship between the energy distributions of the electrons emerging from the electrodes or plates of the parallel plate spectrometer and the current-voltage curve of the spectrometer, the following assumptions will be made:

1. Edge effects are negligible due to the small gap (.25 in.) between the collecting plates compared to the plate diameter (7.0 in.). Furthermore, only the central portion of the plates was irradiated while collection of emitted electrons took place from the total plate area, thus more nearly approximating infinite plane parallel geometry.

2. The number and energy of the electrons emitted from the plates is not altered by the applied collecting voltage (V). Also, the energy distribution is not distorted by any medium between the collecting plates due to the vacuum maintained in the spectrometer ($< 5 \times 10^{-6}$ mm of Hg).
3. Equal numbers of electrons having identical energy distributions are emitted from both upper and lower plates of the spectrometer.

The energy distribution of electrons emitted by the plates may be determined by analyzing the current-voltage curve if the angular distribution of emission is known. The relationship between the energy distribution and the current collected at a given applied voltage may be understood on the basis of the following arguments.

Consider first the parallel plate collecting electrodes when the lower electrode is positive with respect to the upper electrode,

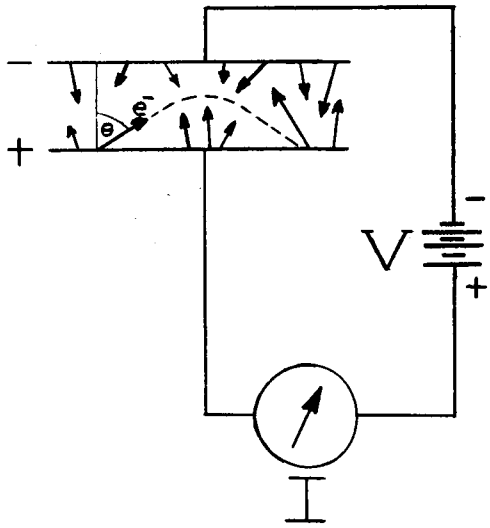

as shown in the sketch. When the lower electrode is positive, all those electrons emitted from upper or negative electrode reach the lower electrode. All those electrons emitted upwards from the lower electrode reach the upper electrode if they have a kinetic energy

(expressed in ev), associated with the component of the velocity perpendicular to the electrode, which is equal to or greater than the applied collecting voltage, V. Therefore, those electrons having kinetic energy, associated with the component of velocity perpendicular to the electrode, which is less than the applied collecting voltage V, will return to the positive lower electrode from which they were emitted. The current which is observed at any particular collecting voltage is thus due to those electrons leaving the negative electrode which are the counterparts of those leaving the positive electrode which have insufficient energy to reach the negative electrode. A reversal of the polarity of the collecting voltage should exactly reverse the current if the emission of electrons from one plate is identical to that from the other.

In order to calculate the total current I, obtained at some collecting voltage V, from a given emitted electron energy distribution, N(V), the angle of emission from the surface of these electrons must be either known or assumed. Since angular emission distributions are not well known, the straight-ahead, isotropic, and cosine distributions will be assumed successively and treated here. Each of these distributions is characteristic of the emission anticipated in some physical situation, and a determination of the relationship between the energy distribution and the derivatives of the current-voltage curve affords an insight into the operation

of the parallel plate spectrometer as well as providing an interesting exercise in the solution of integral equations. For the straight-ahead angular emission assumption, the kinetic energy associated with the velocity component perpendicular to the collecting electrodes is identically the kinetic energy of the electron. Therefore, as seen previously, the current, I, is due to the counter parts from the negative plate of all those electrons leaving the positive electrode which have energy less than the applied collecting voltage V. Therefore, I can be expressed as

$$I = eAR \int_{0}^{V} N(V')dV' \qquad (1)$$

where $N(V')dV'$ is the number of electrons per unit area per roentgen emerging from either electrode, which have an energy between V', and $V'+dV'$, A is the average area of the irradiated electrodes, e is the charge on the electron, R is the dose rate in roentgen/sec., and V, as already mentioned, is the applied collecting voltage.

To obtain $N(V)$, the desired energy distribution, from I, Equation (1) may be differentiated with respect to V and evaluated at the limits of integration which gives

$$\frac{dI}{dV} = eAR\, N(V). \qquad (2)$$

Solving Equation (2) gives N(V) as

$$N(V) = \frac{1}{eAR} \frac{dI}{dV} \quad . \tag{3}$$

For the assumed case of straight-ahead angular emission, it is seen that the number of electrons emerging from either electrode having an energy between V and V+dV (where V is the applied chamber potential) is proportional to the first derivative of the experimental current-voltage curve at the voltage V.

Consider next the case where electrons emerge from the electrode surface isotropically, i.e., the same number per unit solid angle in any direction.

As seen previously, all those electrons which leave the negative electrode will, of course, reach the positive electrode. But only those electrons leaving the positive electrode whose kinetic energy associated with the velocity component perpendicular to the electrode is greater than or equal to the applied voltage, V, will reach the negative electrode. Let v_o be the velocity an electron must have to cross against the field if it is emitted normal to the surface. Then

$$v_o = \sqrt{2ev/m} \tag{4}$$

where e is the charge on the electron, m is the mass of the electron, and V is the applied collecting voltage.

In order for an electron of velocity v emitted at an angle θ to the normal to reach the negative electrode, it must satisfy the condition that

$$v \cos \theta \geq v_o \quad . \tag{5}$$

Let θ_1 be defined as the angle of emission for which an electron of velocity, v, leaving the positive electrode just grazes the negative electrode when the applied voltage is V. Then

$$\cos \theta_1 = \frac{v_o}{v} \quad . \tag{6}$$

Let f be defined as the fraction of all electrons emitted from the positive plate with velocity $v \geq v_o$ which fail to reach the negative electrode. The fraction f can be found by simply integrating the differential solid angle element from θ_1 to $\pi/2$ because of the assumption of isotropic emission. Thus

$$f = \int_{\theta_1}^{\pi/2} \alpha \, 2\pi \sin \theta d\theta \quad , \tag{7}$$

where $2\pi \sin \theta d\theta$ is the differential solid angle, and α is a normalization constant to be determined.

The integral of the angular distribution may be normalized to unity over the direction away from the surface. Thus

$$1 = \int_0^{\pi/2} \alpha\, 2\pi \sin\theta d\theta = \alpha\, 2\pi \tag{8}$$

and the normalization factor α becomes

$$\alpha = \frac{1}{2\pi} \quad . \tag{9}$$

The fraction f may now be evaluated from (9) and (7).

$$f = \int_{\theta_1}^{\pi/2} \sin\theta d\theta = \Big[-\cos\theta \Big]_{\theta_1}^{\pi/2} = \cos\theta_1 \quad . \tag{10}$$

Substituting (6) in (10) gives

$$f = \frac{v_o}{v} \quad . \tag{11}$$

Now the current, I, obtained at an applied collecting voltage V, is composed of the sum of two integrals over the velocity distribution. The first integral is the contribution of the current due to all those electrons with velocity $v \leq v_o$, and the second integral is the current due to that fraction of electrons, f, given by (11), with velocity $v > v_o$. Therefore

$$I = eAR \left[\int_0^{v_o} N(v)dv + \int_{v_o}^{\infty} \frac{v_o}{v} N(v)dv \right] , \tag{12}$$

where $N(v)dv$ is the number of electrons per unit area per roentgen, emerging from either electrode which have a velocity between v and v+dv.

Differentiation of I, given by (12), with respect to v_o and evaluation of the differentiated integrals at their limits yields

$$\frac{dI}{dv_o} = eAR \left[N(v_o) - \frac{v_o N(v_o)}{v_o} + \int_{v_o}^{\infty} \frac{N(v)}{v} dv \right] . \qquad (13)$$

Differentiation of (13) with respect to v_o gives

$$\frac{d^2 I}{dv_o^{\,2}} = eAR \left[- \frac{N(v_o)}{v_o} \right] . \qquad (14)$$

Now (14) can be solved for the velocity distribution $N(v_o)$, giving

$$N(v_o) = - \frac{1}{eAR} \, v_o \frac{d^2 I}{dv_o^{\,2}} . \qquad (15)$$

To obtain the desired energy distribution, N(V), the proper conversion from the velocity distribution $N(v_o)$ given in (15) must be made. The velocity energy definition (4) may be written as

$$eV = 1/2 \, mv_o^{\,2} . \qquad (16)$$

Now solving for V in (16) and differentiating with respect to v_o, it is seen that

$$\frac{dV}{dv_o} = \frac{1}{2e} \; 2 \, mv_o = \frac{mv_o}{e} \quad . \tag{17}$$

Substitution of (4) in (17) gives

$$\frac{dV}{dv_o} = \frac{m}{e} \sqrt{2eV/m} = \sqrt{2m/e} \quad V^{\frac{1}{2}} \quad . \tag{18-a}$$

Also

$$\frac{dv_o}{dV} = \sqrt{e/2m} \quad V^{-\frac{1}{2}} \tag{18-b}$$

Now

$$\frac{dI}{dv_o} = \frac{dI}{dV} \frac{dV}{dv_o} \quad . \tag{19}$$

Substitution of (18-a) in (19) gives

$$\frac{dI}{dv_o} = \frac{dI}{dV} \sqrt{2m/e} \quad V^{\frac{1}{2}} \quad . \tag{20}$$

Differentiation of (20) with respect to v_o proceeds as follows:

$$\frac{d}{dv_o} \left(\frac{dI}{dv_o} \right) = \left[\frac{d}{dV} \left(\frac{dI}{dv_o} \right) \right] \frac{dV}{dv_o} \quad . \tag{21}$$

Substituting (18-a) and (20) in (21) gives

$$\frac{d^2I}{dv_o^{\,2}} = \left[\frac{d}{dV}\left(\frac{dI}{dV}\sqrt{2m/e}\;\; V^{\frac{1}{2}} \right) \right] \sqrt{2m/e}\;\; V^{\frac{1}{2}} \quad . \tag{22}$$

Completion of the differentiation on the right in (22) gives

$$\frac{d^2I}{dv_o^{\,2}} = \left[\frac{d^2I}{dV^2}\sqrt{2m/e}\; V^{\frac{1}{2}} + \tfrac{1}{2}\, V^{-\frac{1}{2}} \sqrt{2m/e}\;\; \frac{dI}{dV} \right] \sqrt{2m/e}\;\; V^{\frac{1}{2}} \tag{23}$$

or

$$\frac{d^2I}{dv_o^{\,2}} = \frac{2mV}{e}\,\frac{d^2I}{dV^2} + \frac{m}{e}\,\frac{dI}{dV} \quad .$$

The energy distribution $N(V)$ is related to the velocity distribution $N(v_o)$ by

$$N(V)dV = \left[N(v_o)\,\frac{dv_o}{dV} \right] dV \quad . \tag{24}$$

Using the following sequence substitution of (15), (23) and (18-b) in (24), the final result is

$$N(V) = -\frac{1}{eAR}\left[2V\,\frac{d^2I}{dV^2} + \frac{dI}{dV} \right] \quad . \tag{25}$$

Inspection of (25) shows that the energy distribution for the isotropic angular emission assumption is dependent upon both the first and second derivatives of the current voltage curve.

In considering the cosine angular emission assumption, the symbols v_o, α, θ, θ_1 and f will retain the same definitions as given in the isotropic angular emission derivation. Once again only those electrons with a sufficient normal velocity component, $v \cos \theta \geq v_o$, will reach the negative electrode after being emitted from the positive electrode.

The fraction, f, of those electrons with velocity $v \geq v_o$ which leave the positive electrode, but fail to reach the negative electrode will, of course, have a different value from that derived for the isotropic emission case. Using the cosine angular emission assumption, f is now defined.

$$f = \int_{\theta_1}^{\pi/2} \alpha \, 2\pi \sin \theta \cos \theta d\theta = \alpha\pi \int_{\theta_1}^{\pi/2} \sin (2\theta) \, d\theta \quad . \tag{26}$$

Integration of (26) and substitution of (6) $\left[\frac{v_o}{v} = \cos \theta_1 \right]$ gives

$$f = \alpha\pi \left(\frac{v_o}{v} \right)^2 \quad . \tag{27}$$

The normalization constant, α, is obtained from

$$I = \alpha\pi \int_0^{\pi/2} \sin(2\theta)d\theta = \alpha\pi \tag{28}$$

or

$$\alpha = 1/\pi \quad . \tag{29}$$

Substitution of (29) in (27) gives

$$f = \left(\frac{v_o}{v}\right)^2 \quad . \tag{30}$$

Now the current I obtained at some applied voltage V corresponding to the electron velocity v_o, given by (4) is composed of two integrals as in the isotropic emission case. The first integral gives the current due to all those electrons having velocity $v \leq v_o$ and the second integral gives the current due to that fraction, f, of those electrons which have velocity $v > v_o$, therefore,

$$I = eAR \left[\int_0^{v_o} N(v)dv + \int_{v_o}^{\infty} \left(\frac{v_o}{v}\right)^2 N(v)dv \right] \quad . \tag{31}$$

Solving for $N(v_o)$ is accomplished by two differentiations of (31). The first differentiation of (31) with respect to v_o gives

$$\frac{dI}{dv_o} = eAR \left[2v_o \int_{v_o}^{\infty} \frac{N(v)}{v^2} dv \right] \quad . \tag{32}$$

Differentiating (32) with respect to v_o and substituting from (32) gives

$$\frac{d^2I}{dv_o^{\,2}} = \frac{1}{v_o}\,\frac{dI}{dv_o} - 2eAR\,\frac{N(v_o)}{v_o} \quad . \tag{33}$$

Solving (33) for $N(v_o)$,

$$N(v_o) = \frac{1}{2eAR}\left[\frac{dI}{dv_o} - v_o\,\frac{d^2I}{dv_o^{\,2}}\right] \quad . \tag{34}$$

Using the velocity distribution relationship given by (24), substitution of (34) in (24) gives

$$N(V) = \frac{1}{2eAR}\left[\frac{dI}{dv_o} - v_o\,\frac{d^2I}{dv_o^{\,2}}\right]\frac{dv_o}{dV} \quad . \tag{35}$$

Further substitution of (4), (18-b), (23) and (20) in (35) gives as the final result

$$N(V) = -\frac{1}{eAR}\,V\,\frac{d^2I}{dV^2} \quad . \tag{36}$$

From (36) it is seen that the flux of electrons having an energy between V and V+dV where V is the chamber voltage is proportional to the applied voltage and second derivative of the current-voltage curve if the electrons follow a cosine angular emission law.

C. I vs. V for Assumed Energy Distribution

If the energy distribution, N(V), of emerging electrons from a surface is known, then it is very simple to derive a current-voltage equation for these electrons, provided their angular emission distribution is known or can be assumed.

Using Greening's[9] semi-quantitative energy distribution and considering the straight-ahead, isotropic and cosine angular emission distribution, the following current-voltage equations are easily derived for a parallel plate vacuum chamber as shown. The current I obtained for the straight-ahead angular emission is from Equation (1)

$$I = eAR\left[\int_0^V kV'^{\frac{1}{2}}\, e^{-V'/8}\, dV'\right] \text{ for } V \leq 41 \text{ volts},$$

and (37)

$$I = eAR\left[\int_0^{41} kV'^{\frac{1}{2}}\, e^{-V'/8}\, dV' + \int_{41}^{V'} k\,\frac{64}{V'^2}\, dV'\right] \text{ for } V > 41 \text{ volts}$$

where Greening's energy distribution, N(V), is $kV^{\frac{1}{2}}e^{-V/8}$ for electron energies $\leq$ 41 ev and $k\,\frac{64}{V^2}$ for electron energies > 41 ev, A is the average plate area, R is the dose rate, and e is the electronic charge.

For the isotropic angular emission distribution, some fraction, f, given by (11) of those electrons with velocity $v \geq v_o$ contribute to the net electron flow, while for $v < v_o$ all electrons contribute to the net electron flow.

---

[9] Greening, J. R., op. cit.

Let

$$v = \sqrt{2eV'/m} \quad . \tag{38}$$

Substituting (4) and (38) into (11) gives

$$f = \frac{v_o}{v} = \frac{\sqrt{2eV/m}}{\sqrt{2eV'/m}} = \sqrt{V/V'} \quad . \tag{39}$$

Therefore, the current I obtained for the isotropic angular emission using Greening's energy distribution is

$$I = eAR\left[\int_0^V kV'^{\frac{1}{2}}e^{-V'/8}\,dV' + \int_V^{41}\sqrt{V/V'}\;kV'^{\frac{1}{2}}e^{-V'/8}\,dV' + \int_{41}^{\infty}\sqrt{V/V'}\;k\,\frac{64}{V'^2}\,dV'\right] \tag{40}$$

when the applied voltage, V, is ≤ 41 volts. The current, I, obtained when the applied voltage, V, is > 41 volts, is

$$I = eAR\left[\int_0^{41} kV'^{\frac{1}{2}}e^{-V'/8}\,dV' + \int_{41}^{V} k\,\frac{64}{V'^2}\,dV' + \int_V^{\infty}\sqrt{V/V'}\;k\,\frac{64}{V'^2}\,dV'\right] . \tag{41}$$

For the case of the cosine angular emission, the fraction f given by Equation (30) was expressed in terms of v_o and v. In terms of energy and applied voltage f may be obtained by substituting (4) and (38) into (30) as follows

$$f = \left(\frac{v_o}{v}\right)^2 = \frac{V}{V'} \quad . \tag{42}$$

The current, I, obtained using Greening's energy distribution for the cosine angular emission distribution is then

$$I = eAR\left[\int_0^V kV'^{\frac{1}{2}}e^{-V'/8}dV' + \int_V^{41} k\,\frac{V}{V'}\,V'^{\frac{1}{2}}e^{-V'/8}dV' + \int_{41}^{\infty} k\,\frac{V}{V'}\,\frac{64}{V'^2}\,dV' \right] \qquad (43)$$

when the applied voltage, V, is $\leq$ 41 volts. When the applied voltage, V, is > 41 volts, the current, I is then

$$I = eAR\left[\int_0^{41} kV'^{\frac{1}{2}}e^{-V'/8}dV' + \int_{41}^{V} k\,\frac{64}{V'^2}\,dV' + \int_V^{\infty} k\,\frac{V}{V'}\,\frac{64}{V'^2}\,dV' \right] . \qquad (44)$$

D. Energy Spectrum in Medium

In the discussion of the parallel plate spectrometer theory, Section B, it was seen that the energy distribution of the emitted electrons could be found from the current-voltage curve provided their angular emission distribution was known. Since angular emission distributions of emitted electrons are not known with precision and are in general not of the simple forms discussed, the final calculated energy distributions are somewhat open to question as to their validity. Furthermore, the primary interest in the work presented here is the energy spectrum inside the medium. Therefore, a relationship will now be derived which gives the energy distribution that the electrons have

inside the medium before they overcome the surface work function and emerge from the spectrometer plates.

Inside the medium the generated electrons will be assumed to have an isotropic angular distribution. Therefore, the number of electrons $N(E_i)dE_i$ per unit area per roentgen inside the medium which have an energy between E_i and E_i+dE_i multiplied by the differential solid angle $d\Omega_i$ is

$$N(E_i)dE_i d\Omega_i = 2\pi N(E_i)dE_i \sin\theta_i \, d\theta_i \quad . \tag{45}$$

The energy, E_i, of the electron inside the medium is

$$E_i = E_w + E_o \tag{46}$$

where E_w is the minimum constant energy which an electron must have in order to escape from the medium, and E_o is the energy which the emitted electron has outside the medium. In the case of metals, E_w is the sum of the Fermi energy E_F and the photoelectric work function ϕ.

Since the velocity component parallel to the spectrometer plates is the same for a given electron inside and outside the medium, then

$$v_i \sin\theta = v_o \sin\theta_o \quad , \tag{47}$$

where v_i is the velocity inside and v_o is the velocity outside.

Let

$$E_i = \tfrac{1}{2}mv_i^{\,2} = \tfrac{1}{2}m\left[(v_i\cos\theta_i)^2 + (v_i\sin\theta_i)^2 \right] \tag{48}$$

and

$$E_o = \tfrac{1}{2}mv_o^{\,2} = \tfrac{1}{2}m\left[(v_o\cos\theta_o)^2 + (v_o\sin\theta_o)^2 \right] \tag{49}$$

Substituting (48) and (49) in (46) gives

$$\tfrac{1}{2}m\left[v_i^{\,2}\cos^2\theta + v_i^{\,2}\sin^2\theta_i\right] = E_w + \tfrac{1}{2}m\left[v_o^{\,2}\cos^2\theta_o + v_o^{\,2}\sin^2\theta_o\right] . \tag{50}$$

Substitution of the equality (47) and (50) and further simplification using (48) and (49) gives

$$E_i \cos^2\theta_i = E_w + E_o \cos^2 \theta_o \quad . \tag{51}$$

Solving (51) for $\cos \theta_i$ yields

$$\cos \theta_i = \frac{1}{\sqrt{E_i}} \sqrt{E_w + E_o \cos^2 \theta_o} \quad . \tag{52}$$

Differentiation of (52) yields

$$\sin\theta_i d\theta_i = \frac{1}{\sqrt{E_i}} \frac{E_o\cos\theta_o\sin\theta_o d\theta_o}{\sqrt{E_w + E_o \cos^2\theta_o}} \quad . \tag{53}$$

Differentiation of (46) gives

$$dE_i = dE_o \quad . \tag{54}$$

Substitution of (53), (54), and (46) in (45) gives

$$N(E_i)dE_i d\Omega_i = 2\pi N(E_w+E_o) \frac{E_o dE_o}{\sqrt{E_o+E_w}} \frac{\cos\theta_o \sin\theta_o d\theta_o}{\sqrt{E_w+E_o \cos^2 \theta_o}} \quad . \tag{55}$$

Now if the relation

$$\sqrt{E_o} \cos \theta_o < \sqrt{V} \tag{56}$$

is satisfied, a contribution to the net electron flow between spectrometer plates results. From (56) it is seen that all those electrons having energy $E_o < V$ contribute to the current plus all those electrons with $E_o > V$ whose angle of emission θ_o is large enough such that (56) is satisfied. Therefore, the total current, I, is

$$\begin{aligned} I = eAR\, 2\pi \int_o^V \frac{N(E_w+E_o)}{\sqrt{E_o+E_w}} E_o dE_o \int_o^{\pi/2} \alpha \frac{\cos \theta_o \sin \theta_o d\theta_o}{\sqrt{E_w + E_o \cos^2 \theta_o}} \\ + eAR\, 2\pi \int_V^\infty \frac{N(E_w+E_o)}{\sqrt{E_o + E_w}} E_o dE_o \int_{\cos^{-1}\sqrt{V/E_o}}^{\pi/2} \alpha \frac{\cos \theta_o \sin \theta_o d\theta_o}{\sqrt{E_w+E_o \cos^2 \theta_o}} \quad . \end{aligned} \tag{57}$$

Let

$$\mu = \cos \theta_o \tag{58}$$

and

$$d\mu = -\sin \theta_o \, d\theta_o \quad . \tag{59}$$

Then substitution of (58) and (59) in (57) gives

$$I = eAR \int_o^V \frac{N(E_w+E_o)}{\sqrt{E_o+E_w}} E_o dE_o \int_o^1 \frac{\mu d\mu}{\sqrt{E_w+E_o \mu^2}}$$

$$+ eAR \int_V^\infty \frac{N(E_w+E_o)}{\sqrt{E_o+E_w}} E_o dE_o \int_o^{\sqrt{V/E_o}} \frac{\mu d\mu}{\sqrt{E_w+E_o \mu^2}} \quad . \tag{60}$$

Integration with respect to the μ function gives

$$I = eAR \int_o^V N(E_w+E_o) \frac{dE_o}{\sqrt{E_o+E_w}} \left[\sqrt{E_w+E_o} - \sqrt{E_w}\right]$$

$$+ eAR \int_V^\infty N(E_w+E_o) \frac{dE_o}{\sqrt{E_o+E_w}} \left[\sqrt{E_w+V} - \sqrt{E_w}\right] \quad . \tag{61}$$

Further simplification of (61) gives

$$I = eAR \left[(\sqrt{E_w+V} - \sqrt{E_w}) \int_V^\infty N(E_w+E_o) \frac{dE_o}{\sqrt{E_o+E_w}} \right.$$

$$\left. + \int_o^V N(E_w+E_o) \left(1 - \sqrt{E_w/E_o+E_w}\right) dE_o \right] . \tag{62}$$

Now to solve for the energy distribution, $N(E_w+V)$, (62) must first be differentiated with respect to V and evaluated at the limits of integration giving

$$\frac{dI}{dV} = eAR\left[\frac{1}{2\sqrt{E_w+V}}\int_V^\infty N(E_w+E_o)\frac{dE_o}{\sqrt{E_o+E_w}}\right]. \tag{63}$$

Differentiation of (63) with respect to V gives

$$\frac{d^2I}{dV^2} = eAR\left[-\frac{1}{4(E_w+V)^{3/2}}\int_V^\infty N(E_w+E_o)\frac{dE_o}{\sqrt{E_w+E_o}} - \frac{1}{2\sqrt{E_w+V}}\frac{N(E_w+V)}{\sqrt{E_w+V}}\right]. \tag{64}$$

Substitution of the integral of (63) into (64) yields

$$\frac{d^2I}{dV^2} = eAR\left[-\frac{1}{2(E_w+V)}\frac{1}{eAR}\frac{dI}{dV} - \frac{N(E_w+V)}{2(E_w+V)}\right]. \tag{65}$$

Solving (65) for $N(E_w+V)$ gives

$$N(E_w+V) = \frac{1}{eAR}\left[-2(E_w+V)\frac{d^2I}{dV^2} - \frac{dI}{dV}\right]. \tag{66}$$

Equation (66) may be written also as

$$eN(E_w+V) = \left[-2(E_w+V)\frac{d^2(I/AR)}{dV^2} - \frac{d(I/AR)}{dV}\right]. \tag{67}$$

E. The Saturation Current as a Function of the Parameters α and β.

Of special interest in regard to the energy distributions, is whether or not there is some simple analytic function which will fit these distributions. It is shown later that a function of the form

$$eN(E_w+V) = \frac{\alpha}{(\beta+E_w+V)^2} \tag{68}$$

provides a fit to the energy distribution. One estimate of accuracy of this fit can be obtained by calculating the saturation current density of the chamber. In order to calculate this saturation current, a relationship must be found which allows a determination of the number of electrons emerging from the medium from the number of those found inside. Such a relationship has been given by Wolff[10] and it will be derived here for the sake of completeness.

Consider a differential solid angle in the medium into which are moving electrons having an energy distribution $N(E_i)$. From previous discussions it is evident that only those electrons whose velocity component normal to the spectrometer plates is at least equal to the velocity value $\sqrt{2E_w/m}$ will contribute to electron flow between the plates. Thus the condition

$$v_i \cos \theta_i \geqq \sqrt{2E_w/m}$$

or

$$\theta_i \leqq \cos^{-1} \frac{\sqrt{2E_w/m}}{v_i} = \cos^{-1} \sqrt{E_w/E_i} \tag{69}$$

must be satisfied.

[10] Wolff, P. A., op. cit.

If the energy distribution $N(E_i)$ exists inside the medium, the number, N_o, of these electrons which emerge is given by

$$N_o = \int_0^{\cos^{-1}\sqrt{E_w/E_i}} N(E_i) \frac{2\pi \sin \theta_i d\theta_i}{2\pi} \quad . \tag{70}$$

$N(E_i)$ is the number of electrons inside the medium which have an energy between E_i and E_i+dE_i per cm^2 per unit solid angle.

Integration of (70) gives

$$N_o = -N(E_i) \left[\cos \theta_i \right]_o^{\cos^{-1}\sqrt{E_w/E_i}}$$

or

$$N_o = N(E_i) \left[1 - \sqrt{E_w/E_i} \right] \quad . \tag{71}$$

From (70) it is seen that the fraction, $\frac{N_o}{N(E_i)}$, of those electrons of energy E_i inside the medium which emerge is equal to $\left[1 - \sqrt{E_w/E_i}\right]$.

The current density I(V) in units of esu/cm^2-r obtained at some collecting voltage V is then given by

$$I(V) = \int_0^V eN(E_i)(1-\sqrt{E_w/E_i}\,)\, dE_i = \int_0^V \frac{\alpha}{(\beta+E_w+V)^2}\,(1-\sqrt{E_w/E_i}\,)\, dV \qquad (72)$$

where

$$eN(E_i) = \frac{\alpha}{(\beta+E_w+V)^2} \quad ,$$

$$E_i = E_w+V \ , \quad \text{and } dE_i = dV \ .$$

Integration of (71) gives

$$I(V) = \alpha\left[\frac{1}{\beta+E_w} - \frac{1}{\beta+E_w+V}\right] - \frac{\alpha\sqrt{E_w}}{\beta}\left[\frac{\sqrt{E_w+V}}{\beta+E_w+V} - \frac{1}{\sqrt{-\beta}}\,\mathrm{ctnh}^{-1}\frac{\sqrt{E_w+V}}{\sqrt{-\beta}}\right]$$

$$+ \frac{\alpha\sqrt{E_w}}{\beta}\left[\frac{\sqrt{E_w}}{\beta+E_w} - \frac{1}{\sqrt{-\beta}}\,\mathrm{ctnh}^{-1}\frac{\sqrt{E_w}}{\sqrt{-\beta}}\right] \ . \qquad (73)$$

III. APPARATUS

A. X-Ray Machine

The X-ray machine used was a Westinghouse "Quadrocondex" 250 KVCP. The X-ray tube was a Westinghouse WL 395 having an inherent filtration of 2.5 mm of aluminum. The only further filtration of the X-ray beam before it passed through the spectrometer plates was the .080 inch thick aluminum cover plate of the vacuum system as shown in Figure 1. The distance between the target of the X-ray tube and the center of the test chamber shown in Figure 2 was 35.5 cm (or 14.1 inches). A one-half inch thick lead plate diaphram, shown in Figures 1 and 3, with an inside hole diameter of 4 5/32 inches, served to define the X-ray beam reaching the plates. The X-ray head was placed in position over the vacuum system enclosure as shown in Figure 3.

In order to improve the stability of the output of the X-ray machine, a Sorenson A.C. voltage regulator, Model 15000-25, was used to stabilize the input line voltage. Even with this added stability, erratic fluctuations having magnitudes of up to 1% still existed in addition to a 120 cycle ripple component of 2 to 3%. Also, a long-term drift ranging from 1 to 3% (downward) in the X-ray output was observed during the course of a complete run which generally required from four to six hours.

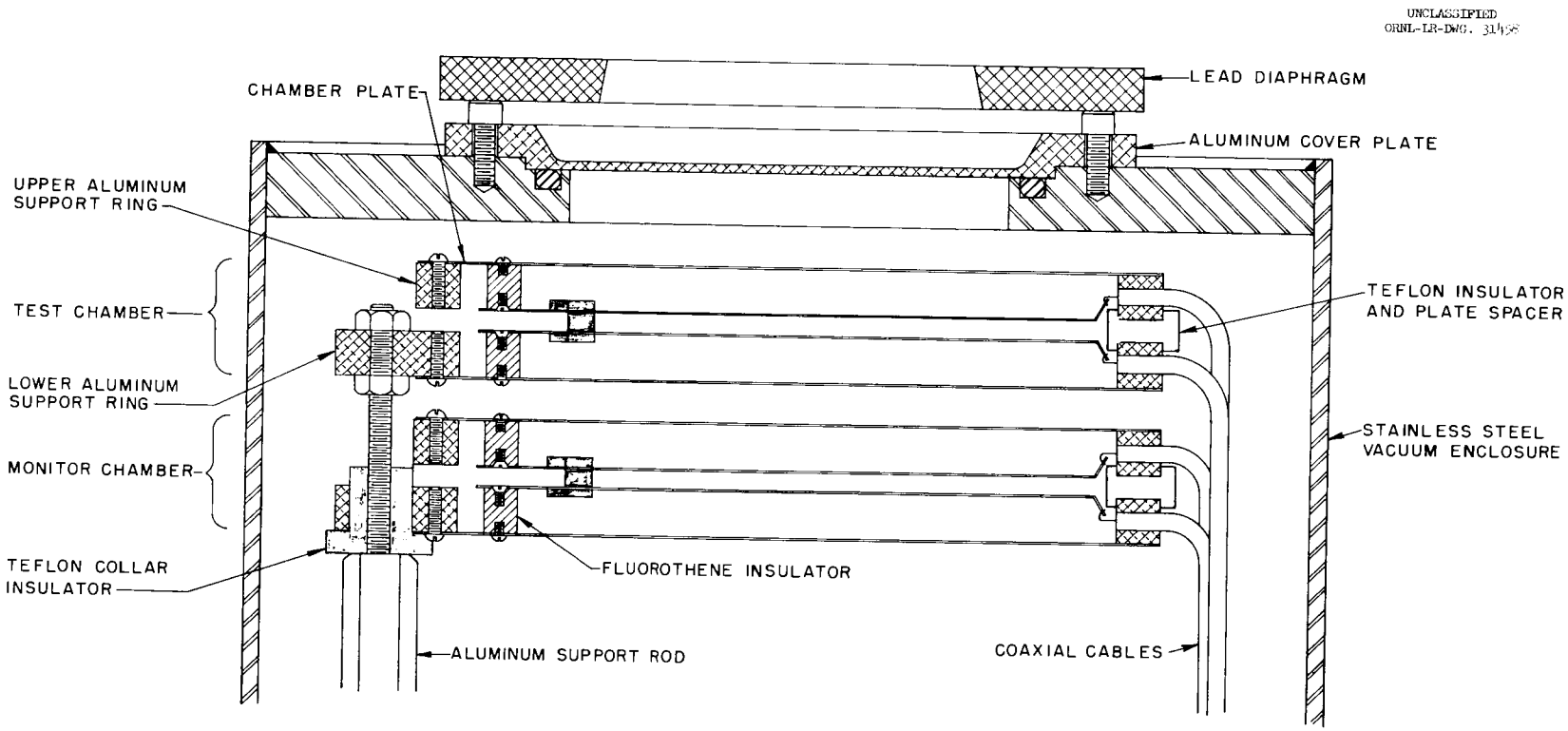

Figure 1. Parallel Plate Spectrometer Cross Section.

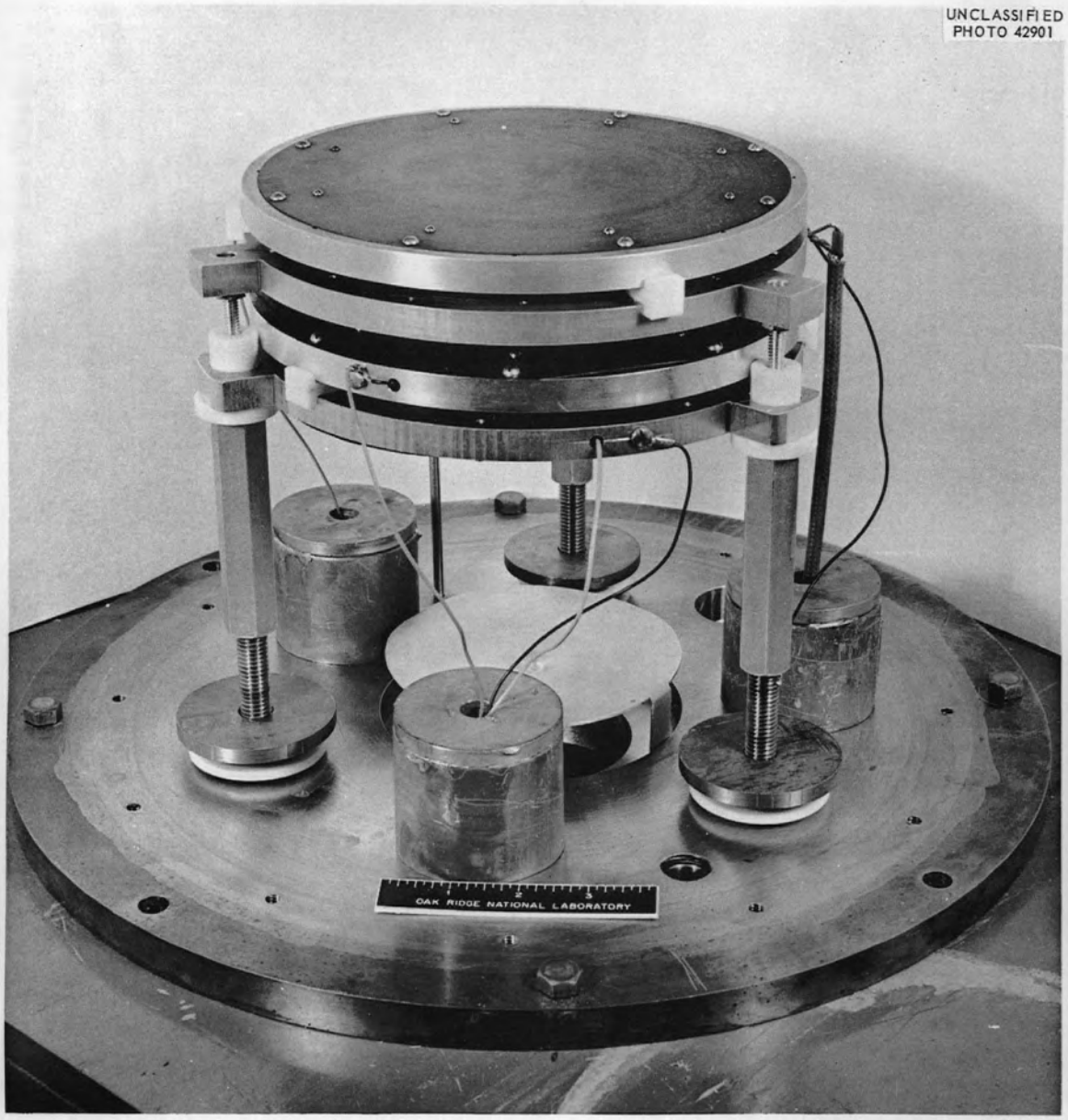

Figure 2. Photograph of Parallel Plate Spectrometer.

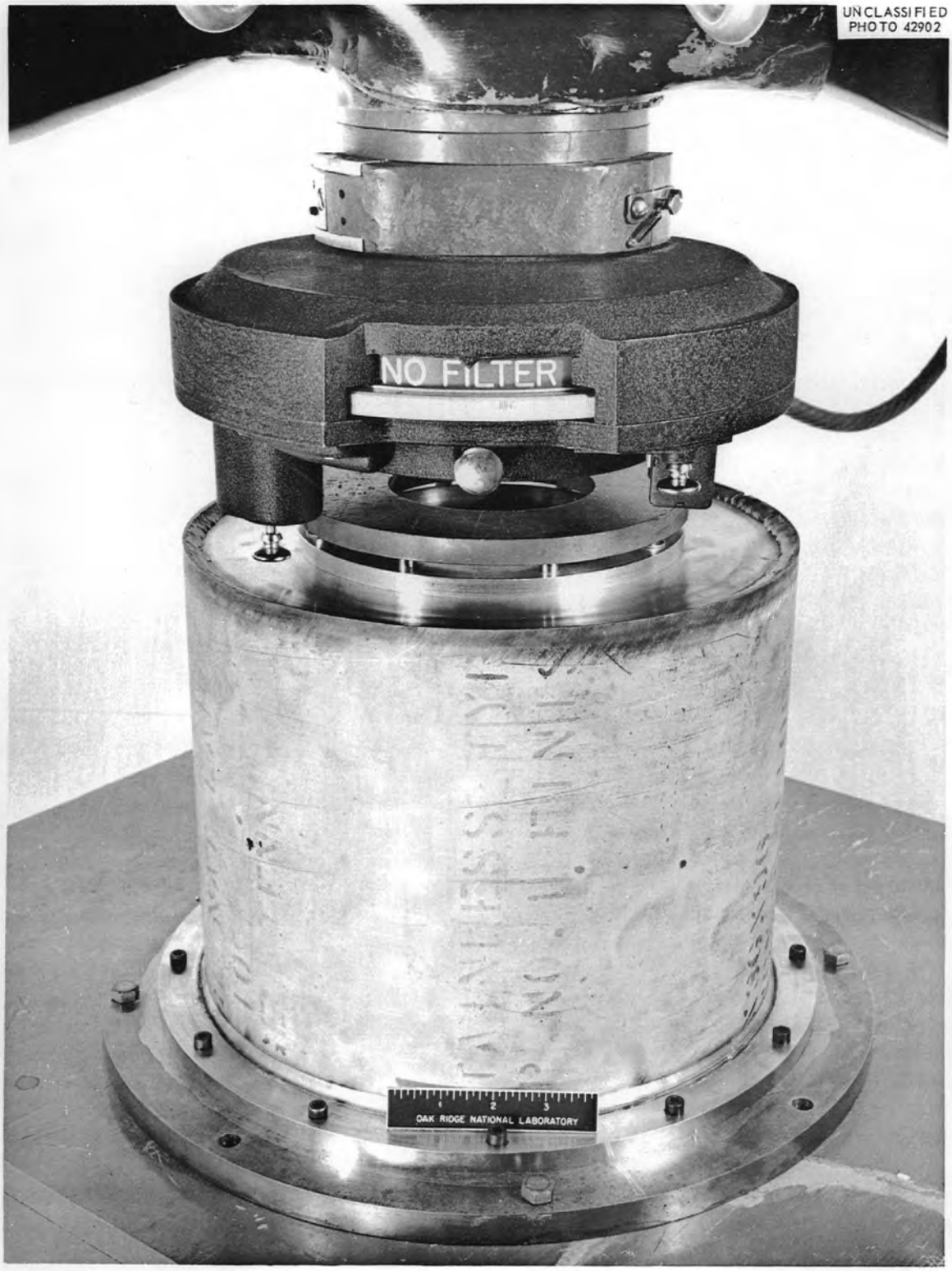

Figure 3. Photograph of X-Ray Head and Vacuum System Enclosure.

It was desirable to measure the current-voltage curve of the vacuum ion chamber to an accuracy of the order of 0.01% in both current and voltage in order that the second derivative of this curve could be calculated to an accuracy of the order of 5%. Thus it was necessary to set up a monitoring chamber as shown schematically in Figure 4. The upper chamber is the test chamber with a variable collecting voltage V and the lower chamber is the X-ray beam monitor with a constant saturation voltage V_M. Since both chambers are in the same X-ray beam, they will both see the same percentage beam fluctuation. Thus, for a given applied voltage V on the test chamber, the ratio I/I_M of the chamber output currents remains constant independent of the beam fluctuation. By reading simultaneously the two currents I and I_M a more precise current-voltage curve for the test chamber could be obtained. One further limitation of the X-ray machine was its maximum current output of 15 ma at 250 kev. In order to improve stability, the current output was reduced to around 10 ma and the output voltage to around 245 kev.

B. Parallel Plate Chambers

Both the test and monitor chambers consisted of four parallel plates. The thickness of the plates for each of the media used was made about equal to the range of a 250 kev electron in that medium.

UNCLASSIFIED
ORNL-LR-DWG. 26474

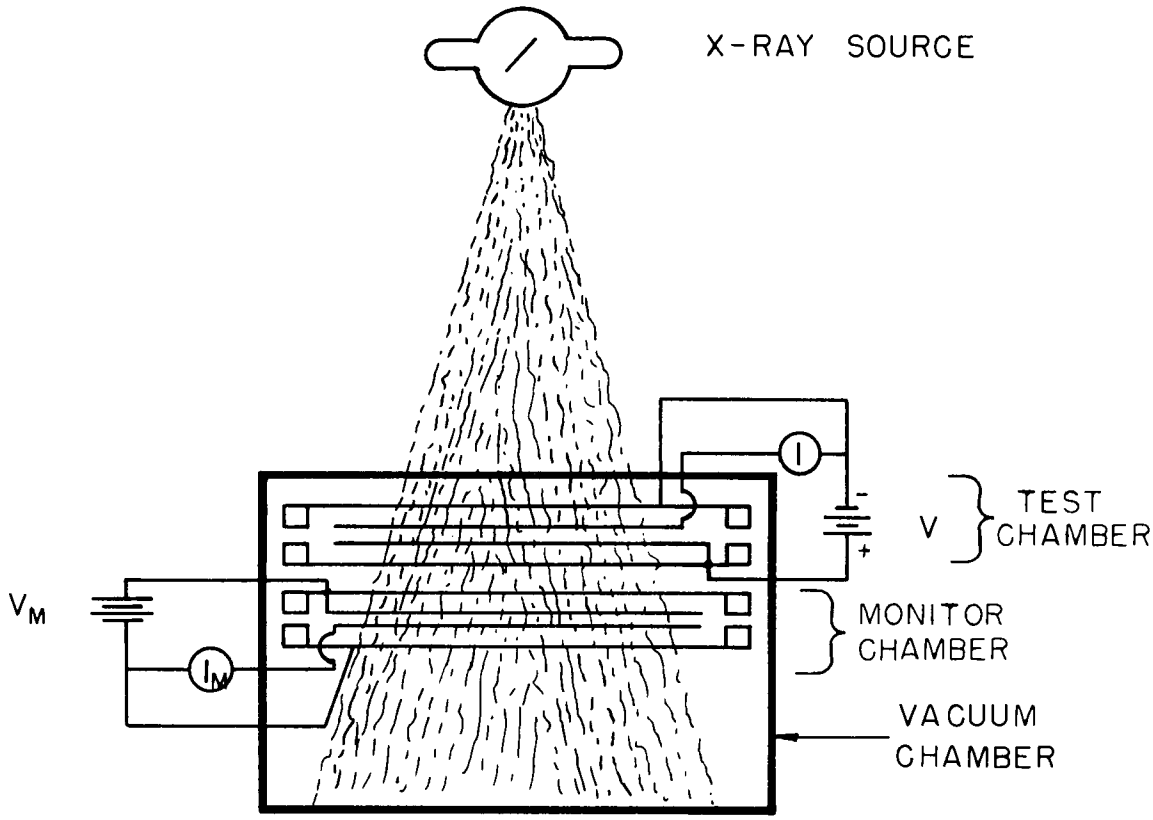

Figure 4. Schematic Diagram of Apparatus.

Theoretical ranges have been given by Spencer[11] and these and the values used here are given in Table I. If the chamber plates were made any thicker, the spectrum of low-energy electrons would probably not be altered appreciable, but the X-ray beam would be attenuated. Therefore, the ideal thickness should be identically equal to the maximum range of the highest energy electrons produced.

Table I. Calculations of Chamber Plate Thickness

Medium	Range (g/cm^2)	Density (g/cm^3)	Ideal Thickness		Thickness Used Inches
			cm	inches	
Copper	.097	8.89	.011	.0043	
a) Chemically Cleaned Surface					.0052
b) Annealed					.0048
Aluminum	.082	2.699	.030	.012	.013
Graphite	.079 *	2.25	.035	.014	.020

* The range used was that given for Beryllium. Because of their close atomic numbers, the value for graphite is approximately the same as that for Beryllium.

The two outer plates of each chamber served two purposes. Referring to Figure 1 and Figure 2, it is seen that the outer plates (8.5 inch diameter) support the inner collecting plates (7.0 inch diameter) by means of eight equally spaced fluorothene

[11] Spencer, L. V., Phys. Rev., 98, 1597 (1955).

insulators (0.495 inches long for Cu, 0.485 for Al, and 0.475 for C) which were tapped for appropriate machine screws. In addition to their role of support, the outer plates had the same applied voltage as the inner collecting electrodes which they supported. Thus unwanted electrons generated elsewhere inside the vacuum system such as those from the aluminum cover plate, base plate, and support rods were stopped from entering the parallel plate spectrometer where they could be collected and add erroneously to the measured current. The outer plates were in turn supported by aluminum rings one-half inch in cross section and having an outside diameter of 8.5 inches with the lower ring being attached to three support rods. The upper and lower rings were then separated by three H-shaped teflon insulators giving a gap of 0.25 inches between the inner collecting plates. Since the test and monitor chambers were suspended by the same three support rods, three inverted T-shaped teflon collars around the support rods served to insulate the monitor chamber from the test chamber.

Copper, aluminum and graphite plates of thicknesses given in Table I were made for the test chamber while the plates of the monitor chamber were made of copper and remained the same throughout all of the current-voltage curve measurements.

An effort was made to remove the oxide layers found on the copper and aluminum plate surfaces in order that any surface effects might be minimized. The copper plates of the monitor chamber were not cleaned however, since its use did not depend on any surface effects. The graphite was not treated in any way since no oxide normally exists and most of the absorbed air out-gassed after the plates were inside the vacuum system for a time.

No practical way of cleaning the copper plate surfaces inside the vacuum system was possible, so a series of chemical cleaning tests were performed on similar copper surfaces outside the system in order to develop a procedure which would leave the surfaces in such a state that they could stand brief exposure to air while being transferred to the vacuum. Although most acids removed the copper oxide, they also removed too much of the copper plates themselves besides leaving the plate surfaces in a state which quickly oxidized again in air. Basic solutions seemed to offer a better cleaning method, and so a buffer solution of one part 1 M NH_4Cl plus five parts 1 M NH_4OH was chosen since these ammonia bases reduce copper oxide readily and do not react with pure copper. After the plates had been immersed for about ten minutes in the heated buffer solution they were rinsed thoroughly in alcohol and immediately placed in the vacuum tank which had been filled with argon. In a matter of minutes the chambers were assembled and the vacuum system pumped

down during which time the plates were continuously in argon. Even though the plates appeared to be clean and shiny after the above cleaning process, later measurements with an Ellipsometer* calibrated for copper gave a value of ~ 150 A° oxide thickness as compared to ~ 300 A° before cleaning. Thus about half of the oxide was probably removed. Another method used for removing copper oxide was to first electropolish the copper specimens and then anneal them at 500° C in an atmosphere of hydrogen. Electropolishing was accomplished using the plate as the anode in an electrolytic cell supplied with current by a Mallory 172 battery charger. Because of the large chamber plate areas and a current limited to 16-17 amp, a slightly etched instead of a mirror-finished surface was obtained. The electropolishing also removed approximately .0005 inch thickness from the plates. The plates were then annealed and a reliable estimate of the probable oxide remaining place the thickness at about ~ 20° A. The hydrogen annealing process also leaves the copper surface in a state which does not easily oxidize even if exposed to normal air.

No straight-forward chemical method was available for removing the oxide layer from aluminum because the aluminum itself reacts more easily with acids and bases than its oxide. Thus a purely mechanical polishing and detergent cleaning technique was used.

* The Ellipsometer Model 436 is designed to give oxide thicknesses for single crystals only. Thus the readings obtained are some sort of average due to the polycrystalline nature and relatively rough surface of the plates. Also, since the instrument is calibrated for a specific oxide, any impurities on the surface can greatly affect its absolute readings.

The final polishing agent used was a sapphire dust, which left the surface shiny and clean in appearance, even if not altogether free of oxide.

C. Electrical System

The various instruments and electronic components used were chosen with particular attention being given to their stability characteristics. Since the expected vacuum chamber currents would be around 10^{-10} amperes in magnitude, a sensitive small-current measuring device was needed. The ORNL Q-826-B electrometer was subsequently chosen because of its good sensitivity and stability. The electrometer is described by Glass[12] and a circuit diagram is shown in Figure 5. As shown in the schematic of Figure 6, each electrometer drives a 10 mv recorder. Each chamber measuring system operates on a null basis with the voltage produced by the chamber currents in R being bucked out by an accurately measured voltage applied to the closed circuit jack in the grid return. The bucking voltages V_R and V_{RM} were supplied by standard 6 and 12 volt wet cells. Rubicon High Precision Type B and Leeds Northrup Type K potentiometers were used to measure one-tenth of the applied bucking voltage with the aid of voltage dividers. Since it was desired to measure the chamber currents or output voltages very accurately, it was necessary that the electrometer grid resistors and the voltage

---

[12] Glass, F. M., Nucleonics, 10, No. 2, 36 (1952).

UNCLASSIFIED
ORNL-LR-Dwg. 7231

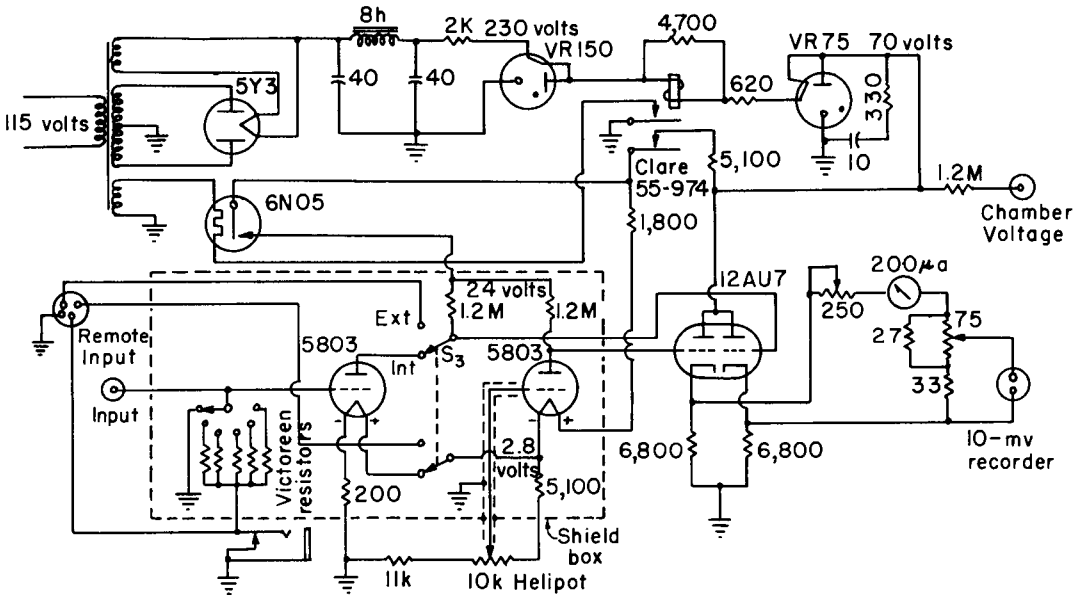

Figure 5. Circuit of the Model Q-826-B Electrometer.

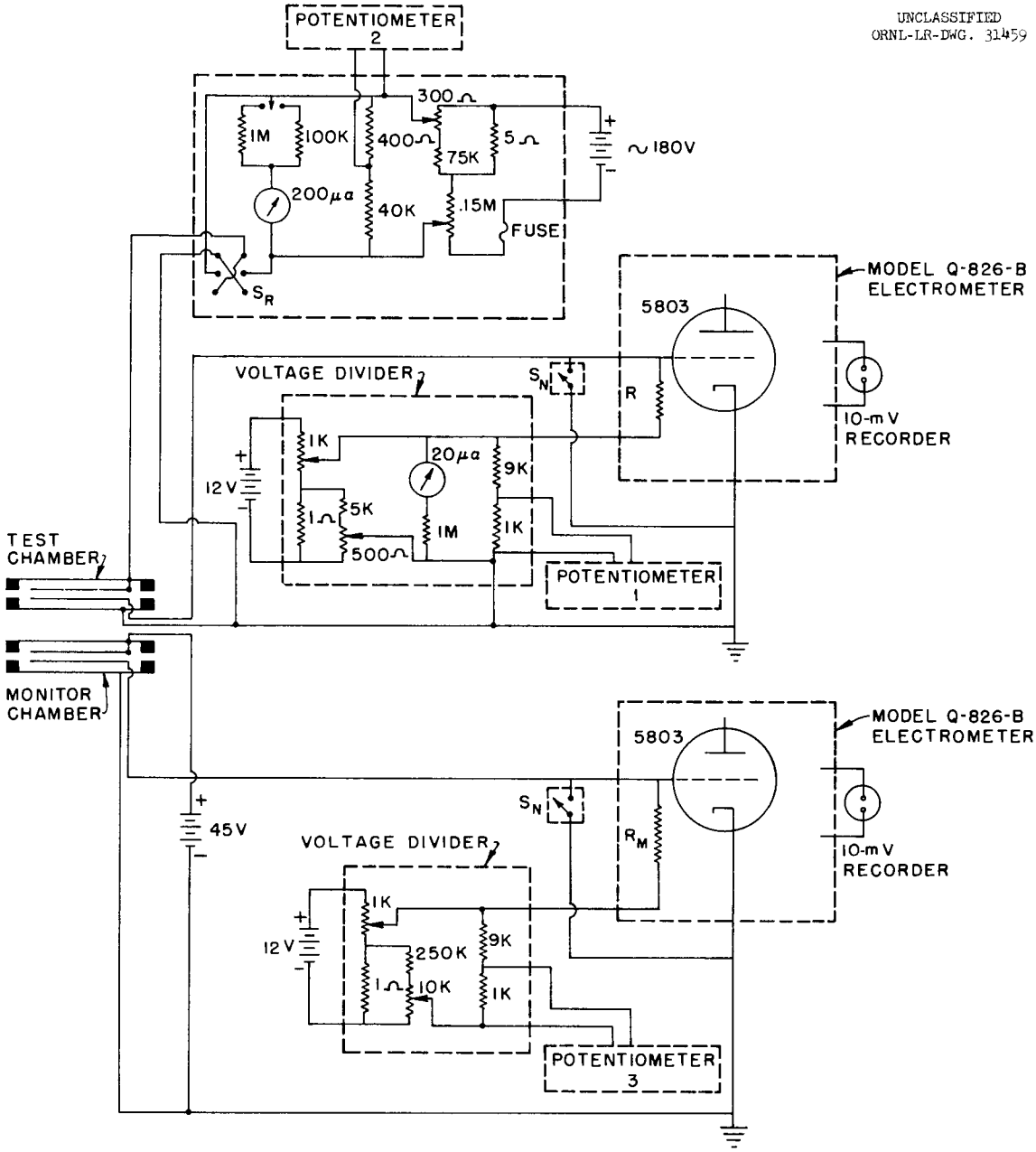

Figure 6. Circuit Schematic.

divider resistors be highly stable. This stability requirement was met in the Q-826-B electrometer by the use of Victoreen precision resistors for the grid resistors R and R_M. Daven precision wire wound resistors were used in the voltage dividers, their tolerance being $\pm$ 0.5% of nominal value and their temperature coefficient only $\pm$ $20/10^6$ per degree Centigrade or $\pm$ 0.002%/C°.

The response time of the electrometer was reduced as much as possible in its design by minimizing stray capacity in the grid circuit. The RC time constant of the input circuit is approximately 0.1 sec for the 10^{10}-ohm range and 1 sec for the 10^{11}-ohm range. The chamber-to-electrometer leads were kept at a minimum length thus introducing as little added capacitance as possible.

The capacity of the parallel plate chambers was about 40 μμf which increased the response time to approximately 0.5 sec for the 10^{10}-ohm range. When the chambers were connected to the leads the final response time became about 1 sec for the 10^{10}-ohm range and 10 sec for the 10^{11}-ohm range. Thus all short-term X-ray fluctuations were effectively integrated in the output current readings while the more important longer-term drifts and changes were detected.

D. Vacuum System

The vacuum system equipment consisted of a Distillation Products Industries diffusion pump, Model MCF 300-01, a Distillation Products Industries water-cooled baffle, a W.M. Welch Manufacturing Company duo-seal vacuum forepump, and a liquid nitrogen vapor trap. A General Electric ion gauge supply was used with a Distillation Products Industries VG 1A ion gauge to measure the vacuum which was maintained in the following ranges for the different media: chemically cleaned copper, $3.4\text{-}3.8 \times 10^{-6}$ mm of Hg; annealed copper, $4.6\text{-}4.8 \times 10^{-6}$ mm of Hg; aluminum, $2.9\text{-}3.0 \times 10^{-6}$ mm of Hg; graphite, $4.0\text{-}4.4 \times 10^{-6}$ mm of Hg. The best vacuums were attained when the diffusion pump was operated at 3.95 amperes and 72 volts. Also the flow of the circulating water coolant in the pump was adjusted such that the water initially at 13° C reached the exit (36 feet of copper tubing from diffusion pump to exit) at a temperature between 22° and 24° C.

IV. EXPERIMENTAL PROCEDURE AND DATA ANALYSIS

Before a complete set of current voltage data was taken for each of the different chambers, a rough current-voltage curve was obtained in order to determine appropriate chamber voltage increments to be used along various portions of the curve. The low voltage region of the current-voltage curve had the largest slope and rate of change of slope. Therefore, small voltage increments were used for the first portion of the curve in order that the derivatives might be evaluated accurately, and larger increments were used as the curve levelled off toward a constant saturation level. The use of too small a voltage mesh was undesirable in that there was a limiting accuracy to which the chamber voltage V could be set. In addition, if successive current measurements had very small differences in their values, the first and second derivatives could once more become meaningless.

The chamber voltage V was measured with a Rubicon High Precision Type B (Pot. 2) potentiometer which actually read 0.99% of V. The bucking voltages were then adjusted until both the electrometer simultaneously gave null readings. Then the applied bucking voltages were read with the Leeds and Northrup (Pot. 1) and Rubicon (Pot. 3) potentiometers. The limiting accuracy of these bucking voltage readings was determined by the smallest bucking voltage increment detectable on the 10 mv recorders, which

will be discussed later in the error analysis in Appendix II. Since the electrometers had a small inherent drift in their zero current position, this zero position was checked with the nulling switches S_n shown in Figure 6 at each reading in the following manner. After the bucking voltages had been adjusted to give a supposedly null current reading, both nulling switches S_n of the two electrometers were closed simultaneously. If no deflection occurred in either electrometer then the bucking voltages were correctly adjusted.

Analysis of this data to obtain the energy distribution centered around the calculations of the first and second derivatives of the current-voltage curve as required by the energy distribution given by Equation (67). The first derivative, $\frac{d(I/AR)}{dV}$ or slope of the current-voltage curve can be expressed

$$\left(\frac{d(I/AR)}{dV}\right)_{\frac{V_{i+1}+V_i}{2}} = \frac{y_{i+1}-y_i}{\Delta \underline{x}} \tag{74}$$

where the derivative is evaluated at $\frac{V_{i+1}+V_i}{2}$, $\Delta \underline{x} = (V_{i+1}-V_i)$ represents the voltage mesh, and y_i is equal to the current per unit area per dose rate $(I/AR)_i$ obtained at an applied chamber voltage V_i.

Now the second derivative, $\frac{d^2(I/AR)}{dV^2}$ of the current-voltage curve is equal to the slope of the $\frac{d(I/AR)}{dV}$ vs V curve. Normally the second derivative would then be expressed

$$\left(\frac{d^2(I/AR)}{dV^2}\right)_{V_{i+1}} = \frac{\frac{y_{i+2}-y_{i+1}}{\Delta X} - \frac{y_{i+1}-y_i}{\Delta X}}{\Delta X}$$

or

$$\left(\frac{d^2(I/AR)}{dV^2}\right)_{V_{i+1}} = \frac{y_{i+2}-2y_{i+1}+y_i}{\Delta X^2}, \tag{75}$$

where the second derivative is evaluated at V_{i+1}. But it can be seen from Equation (75) that if the y_{i+1} current value is in error, the net effect upon the second derivative is far greater than if either y_{i+2} or y_i were in error. Therefore, in order that the current values y_i used in calculating the second derivative might all be weighted equally, four current values were used in the second derivative calculations. The resultant second derivative $\frac{d^2(I/AR)}{dV^2}$ then has the algebraic form

$$\left(\frac{d^2(I/AR)}{dV^2}\right)_{\frac{V_{i+2}+V_{i+1}}{2}} = \frac{y_{i+3}-y_{i+2}-y_{i+1}+y_i}{2\,\Delta X^2} \tag{76}$$

where it is evaluated at

$$\frac{V_{i+2}+V_{i+1}}{2} \quad .$$

Equations (74) and (76) were used in calculating the derivatives as required by Equation (67). Appendix I gives a sample calculation of one point on an energy distribution and Table II tabulates the step by step results for a portion of the annealed copper data.

V. EXPERIMENTAL RESULTS

A comparison of the current-voltage curves obtained from Greening's energy distribution for the isotropic, cosine and straight-ahead emission cases as given by Equations (40), (43) and (37) respectively is made in Figure 7. All three curves become asymptotic to the same current value of 21.20 in arbitrary units at an infinite collecting voltage. Since it became apparent that only Greening's isotropic current-voltage curve would come close in general shape to the experimental curves of this work, comparison was made only to this curve. Figures 8, 9 and 10 show the results of the annealed copper, aluminum and graphite current-voltage curves respectively normalized at 40 volts to Greening's isotropic current-voltage curve. It is readily seen in Figures 8, 9 and 10 that the experimental curves rise nearer their saturation levels at lower collecting voltages than does Greening's isotropic case current-voltage curve. This indicates that the experimental curves have a larger relative number of low energy electrons contributing to the current than does Greening's distribution.

The question of which one of the angular emission assumptions most closely approximates the actual experimental electron emission may be considered. Most experimental secondary emission work seems to indicate that the cosine emission distribution is the best approximation.[13] However, a comparison of the experimental current-voltage

---

[13] McKay, K. G., op. cit.

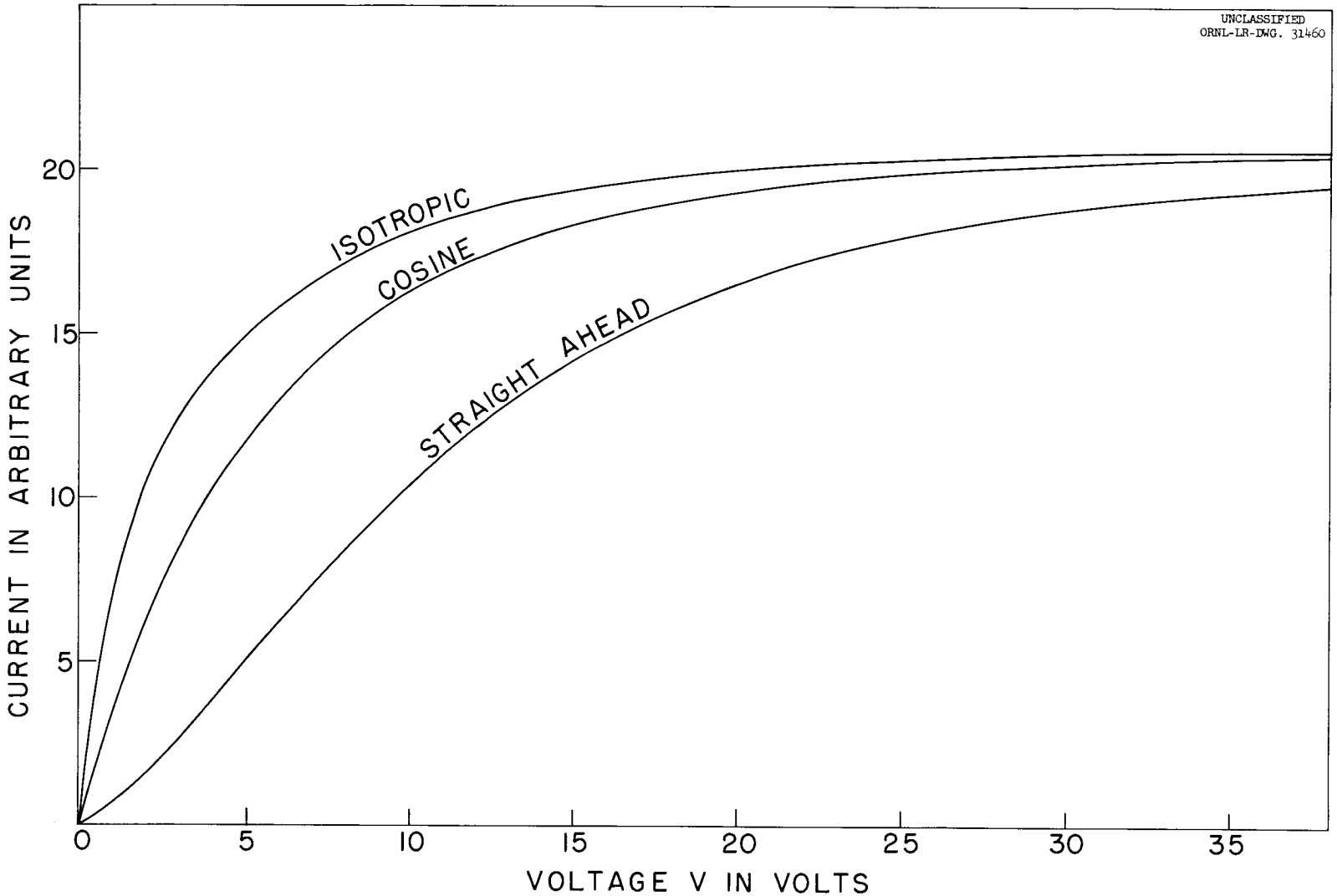

Figure 7. Straight Ahead, Isotropic and Cosine Emission Current-Voltage Curves Assuming Greening's Energy Distribution.

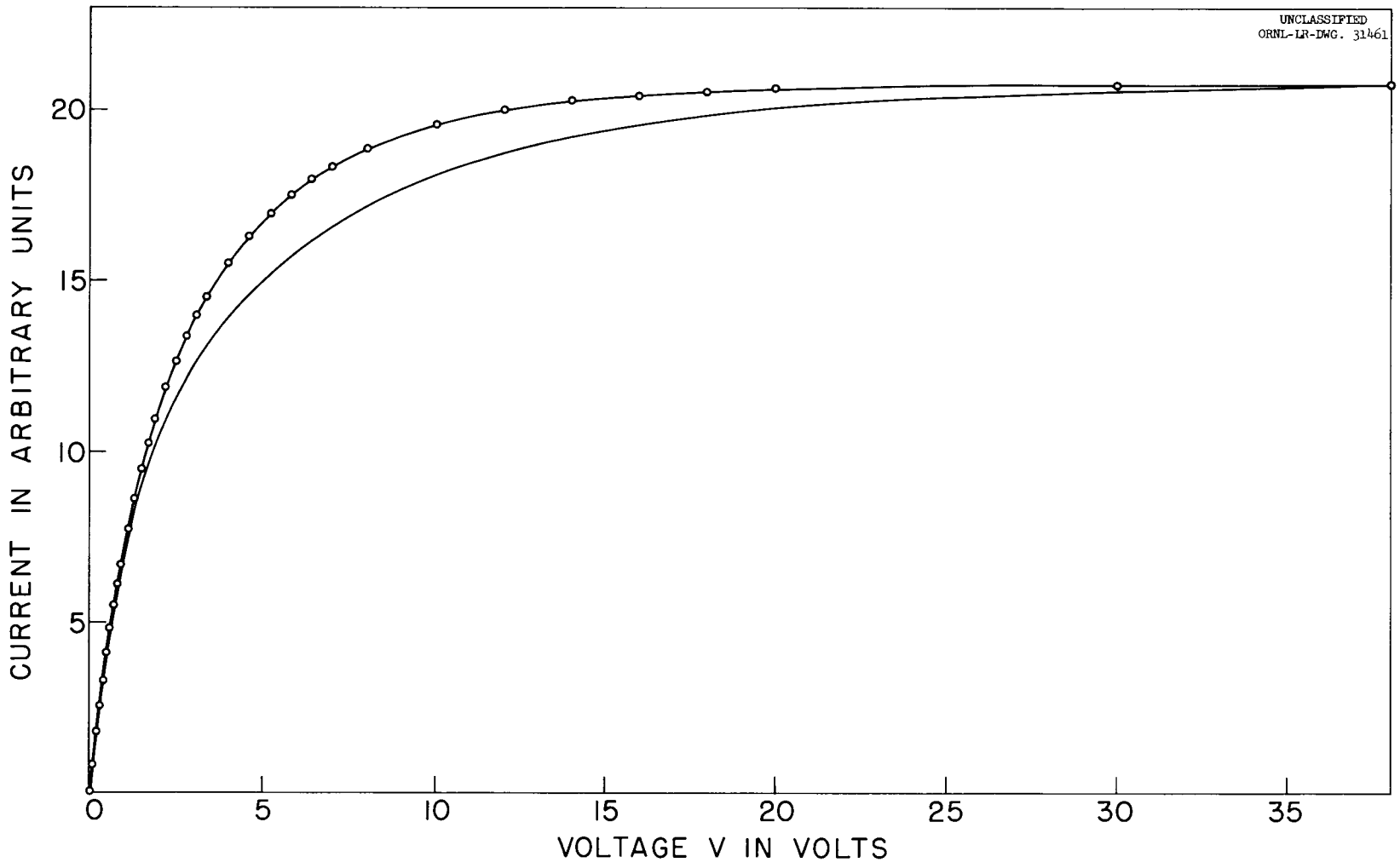

Figure 8. Current-Voltage Curves for Annealed Copper and for Greening's Isotropic Distribution.

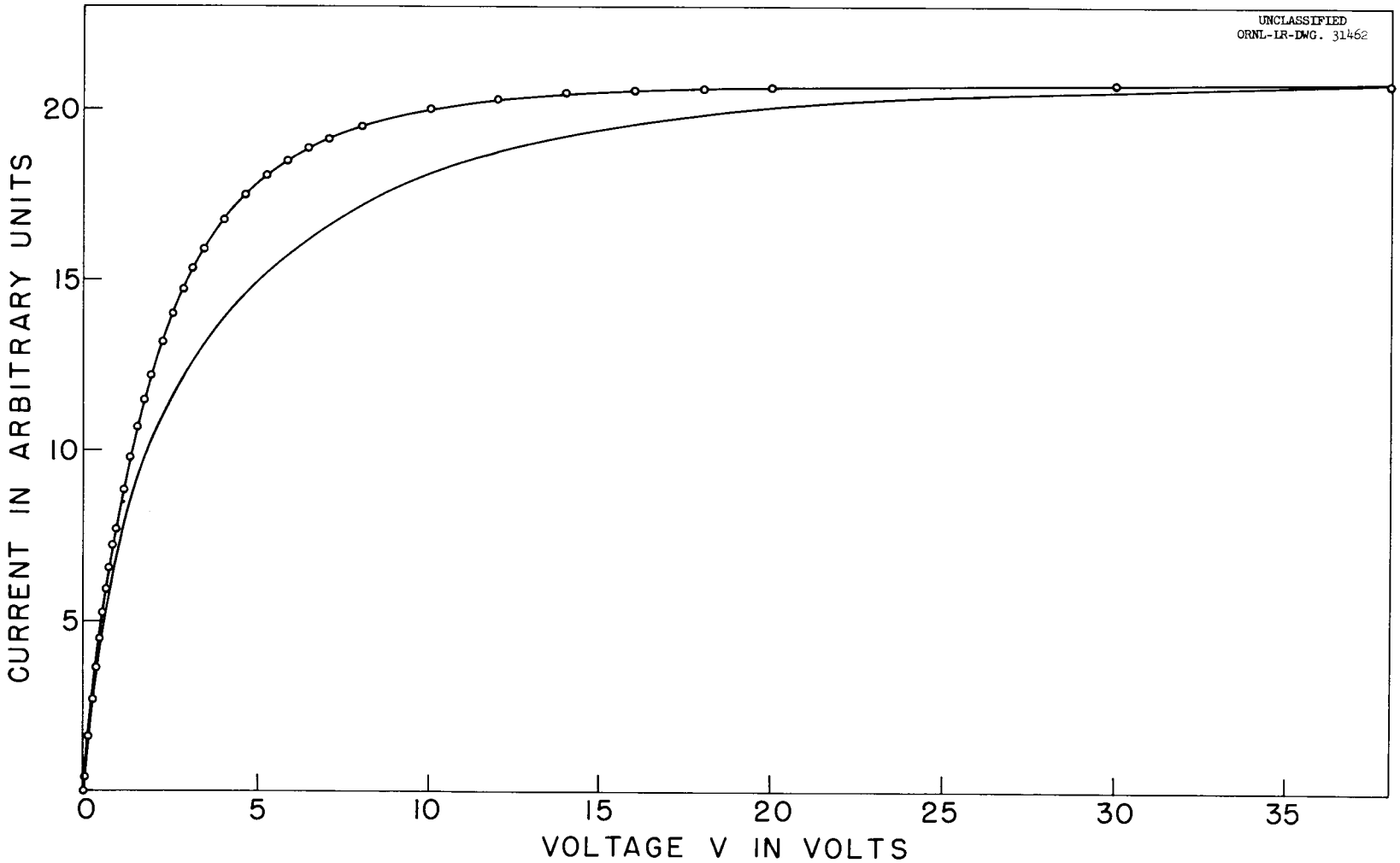

Figure 9. Current-Voltage Curves for Aluminum and Greening's Isotropic Distribution.

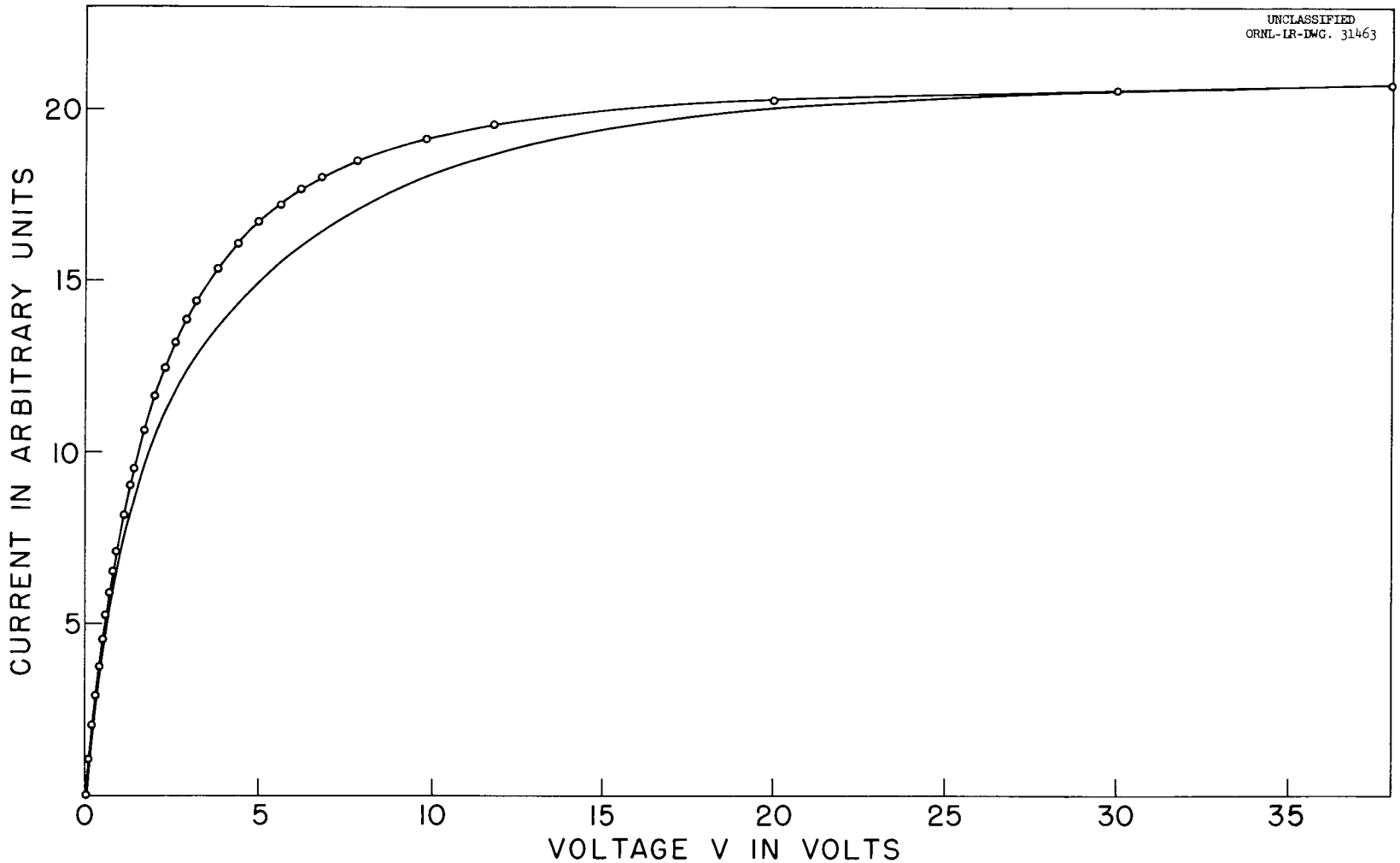

Figure 10. Current-Voltage Curves for Graphite and Greening's Isotropic Distribution.

curves with Greening's corresponding cosine based current-voltage curve would show even larger discrepancies than those observed in Figures 8, 9 and 10 which compare the experimental data of this work with Greening's isotropic current-voltage curve.

From these comparisons and consideration it is therefore evident that the electron energy distributions which contributed to the measured current-voltage curves of this work had a considerably lower energy distribution than that predicted by Greening.

As might be expected, the surface conditions of the spectrometer plates had a definite effect upon the measured current-voltage curves and the calculated energy distributions. Figure 11 compares current-voltage curves of three different copper surfaces normalized to the same ordinate at saturation to facilitate comparison of shapes. In addition to the faster rise of the less-clean copper plates, i.e., thicker oxide layer, the saturation current from these surfaces was also larger. Thus the thicker the oxide layer on the spectrometer plates the larger the saturation current and the lower in average energy the corresponding energy distribution becomes.

A comparison of saturation current values for the different spectrometer plates with values obtained by Taylor[14] is shown in Table II.

---

[14] Taylor, L. S., op. cit.

Table II. Experimental Current Densities

Medium	Experimental Current Density at Chamber Potential of 30 Volts (Saturation)	Values Found By Taylor (Plate Area Assumed to be 60 cm^2)	Values Derived From Empirical Constants α and β
Chemically Cleaned Copper	.0076 $\frac{esu}{cm^2\text{-}r}$		.0086 $\frac{esu}{cm^2\text{-}r}$
Annealed Copper	.0063 $\frac{esu}{cm^2\text{-}r}$		.0064 $\frac{esu}{cm^2\text{-}r}$
Brass		.0028 $\frac{esu}{cm^2\text{-}r}$	
Aluminum	.0011 $\frac{esu}{cm^2\text{-}r}$	.0008 $\frac{esu}{cm^2\text{-}r}$	.0013 $\frac{esu}{cm^2\text{-}r}$
Graphite	.00024 $\frac{esu}{cm^2\text{-}r}$	.00027* $\frac{esu}{cm^2\text{-}r}$	.00025 $\frac{esu}{cm^2\text{-}r}$

* This value is for graphite-coated bakelite.

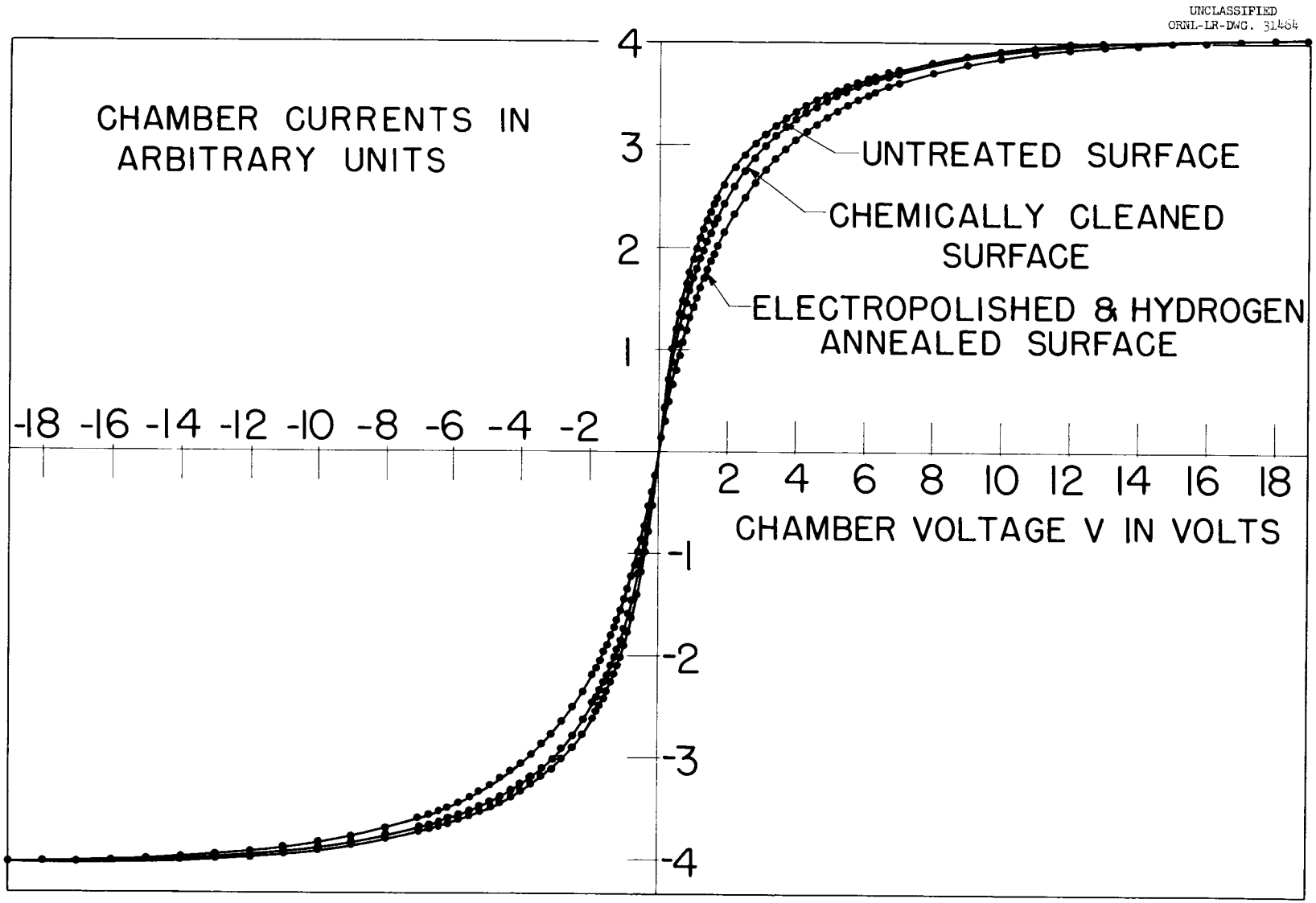

Figure 11. Comparison of Current-Voltage Curves for Three Copper Surfaces.

Figure 12 shows the experimental current-voltage curve of the chemically cleaned copper for a chamber collecting voltage from zero to 70 volts. Since the current levels off after a collecting voltage of 20 volts is reached, the first and second derivatives of this curve become very small, approaching zero. Since the significant portions of the current-voltage curves being analyzed lie within the first twenty volts of the chamber collecting voltage, only this portion will be shown in the remaining current-voltage curve figures.

Appendix I gives the procedure and a sample calculation for obtaining the first and second derivatives of the current-voltage curves and the energy distributions. Figure 13 shows the experimental current-voltage curve and Figures 14 and 15 show the calculated first and second derivatives versus voltage curves for the chemically cleaned copper spectrometer plates.

Figures 16, 17 and 18 show the experimental current-voltage curve and the calculated first and second derivatives versus voltage curves, respectively, for the annealed copper spectrometer plates. Similarily, Figures 19 through 24 show the experimental current-voltage curve and first and second derivatives versus voltage curves, respectively, for aluminum and graphite.

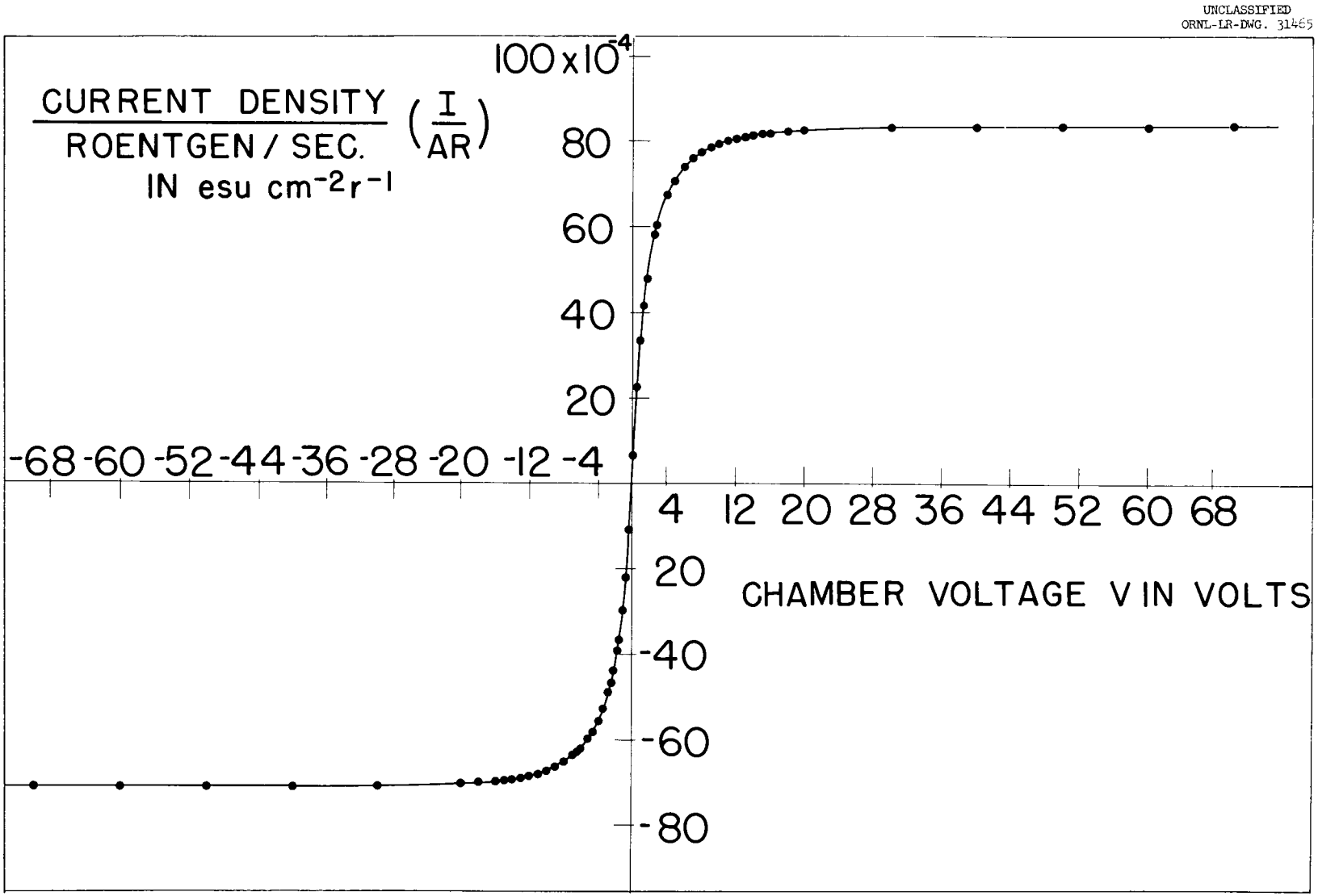

Figure 12. Current-Voltage Curve for Chemically Cleaned Copper.

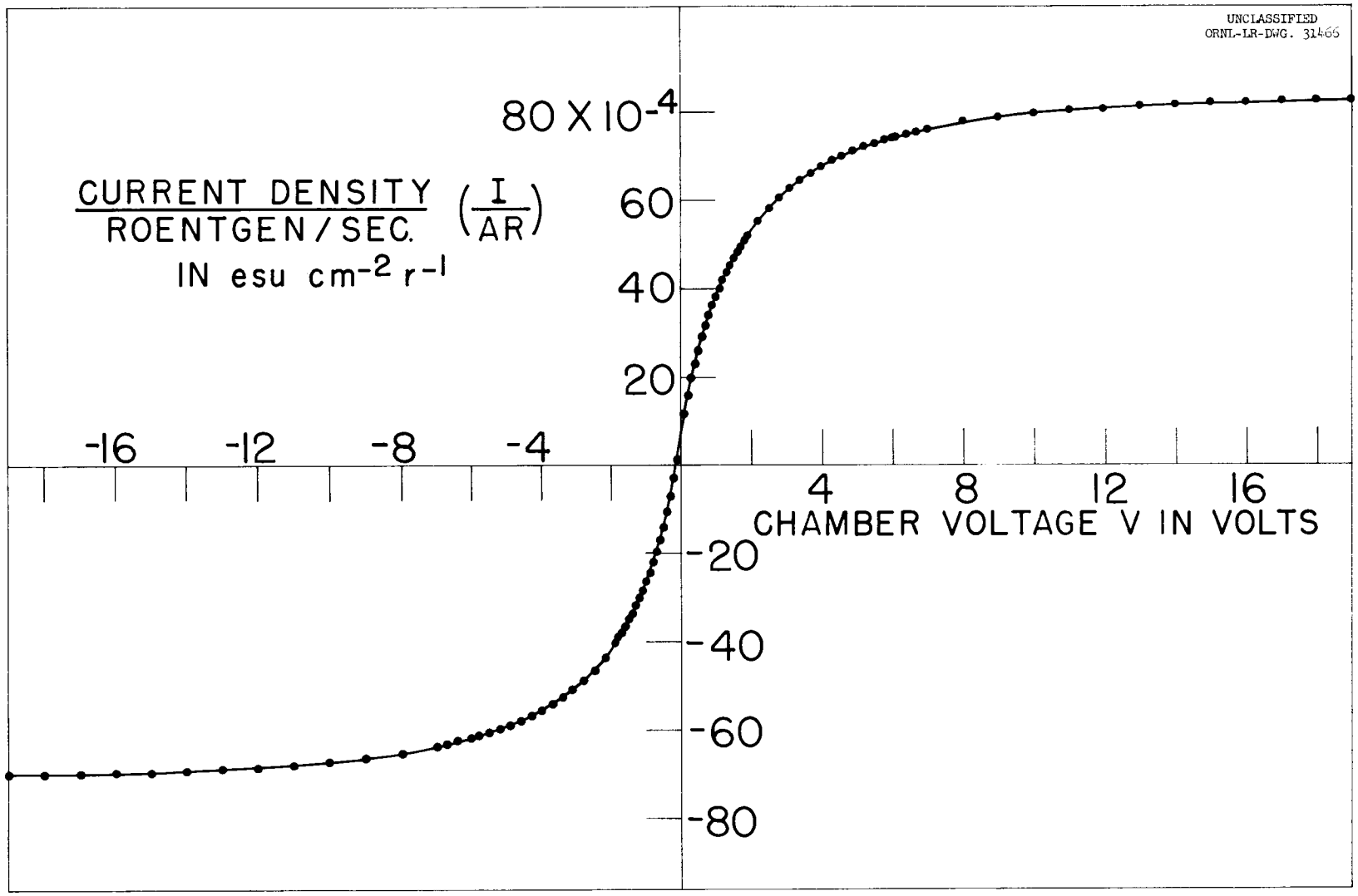

Figure 13. Low Voltage Portion of Current-Voltage Curve for Chemically Cleaned Copper.

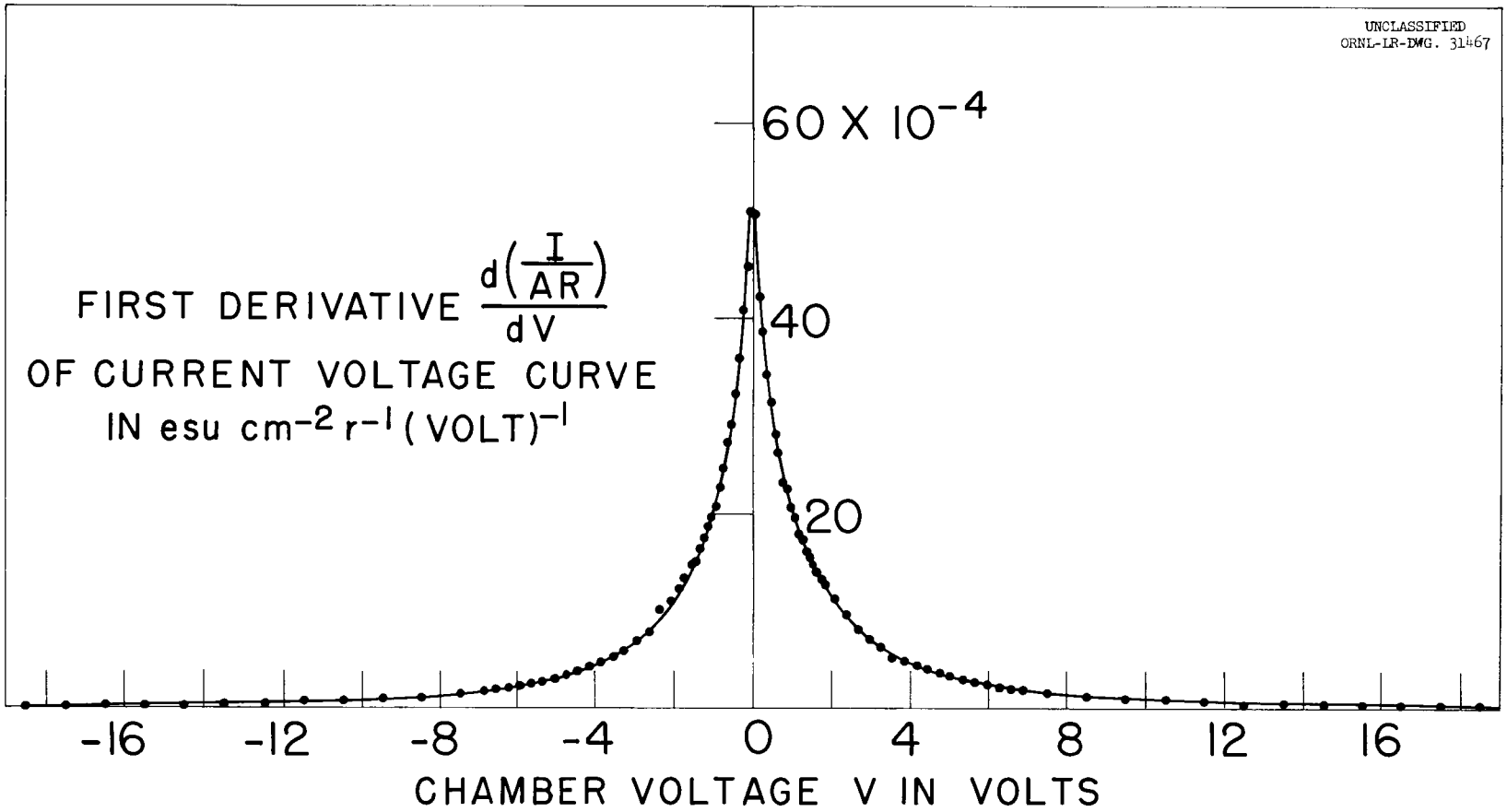

Figure 14. First Derivative of Current-Voltage Curve for Chemically Cleaned Copper.

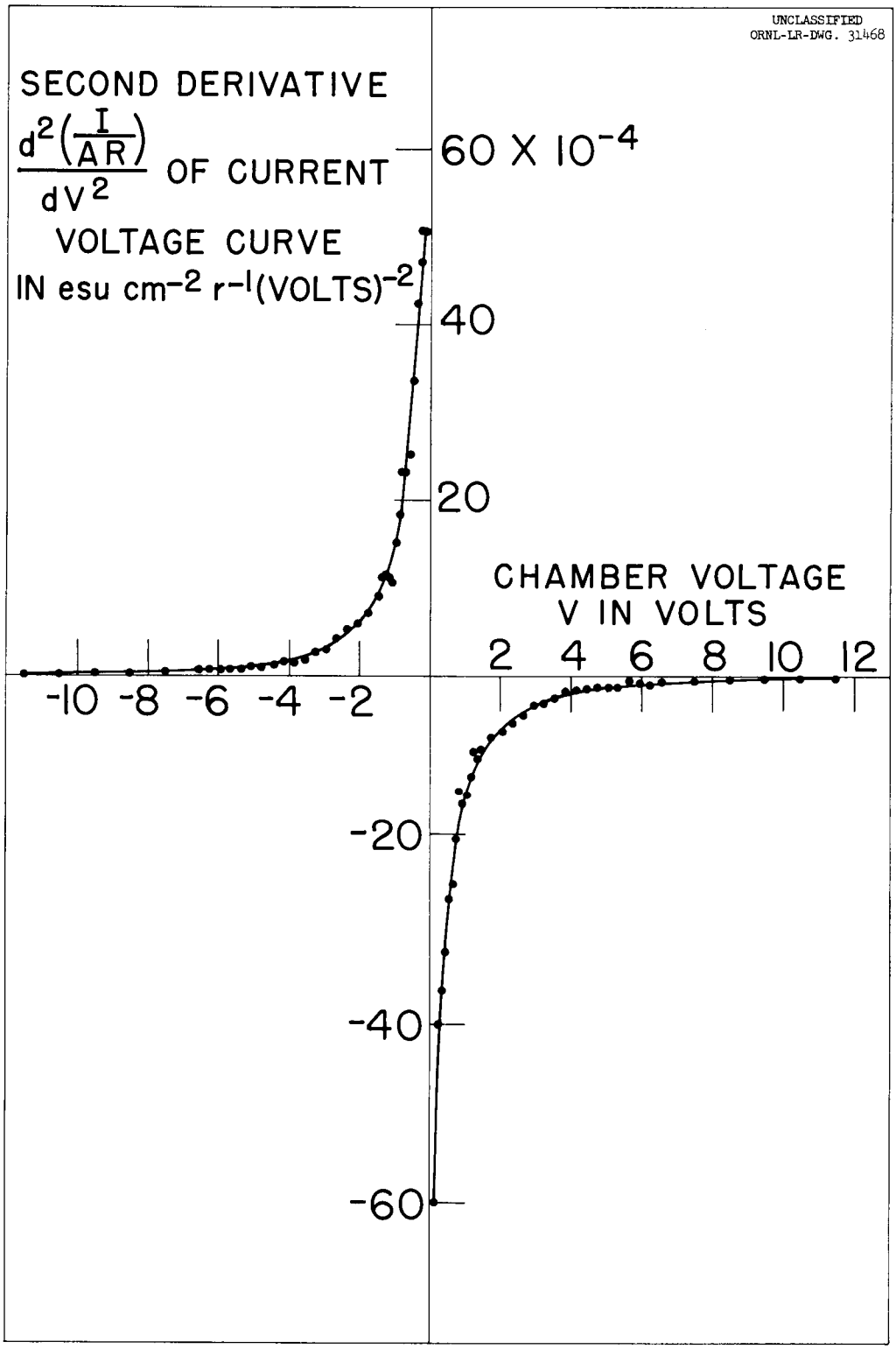

Figure 15. Second Derivative of Current-Voltage Curve for Chemically Cleaned Copper.

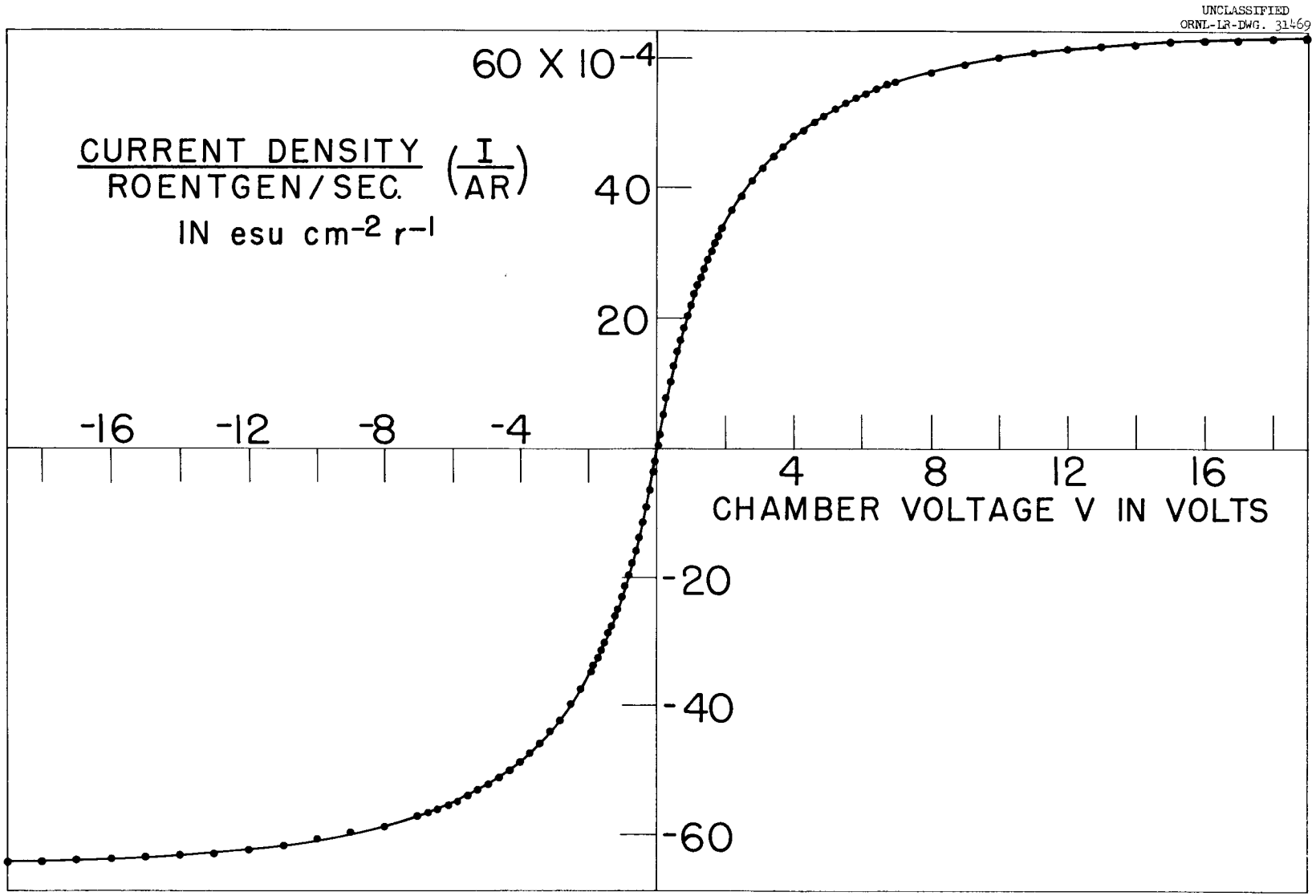

Figure 16. Current-Voltage Curve for Annealed Copper.

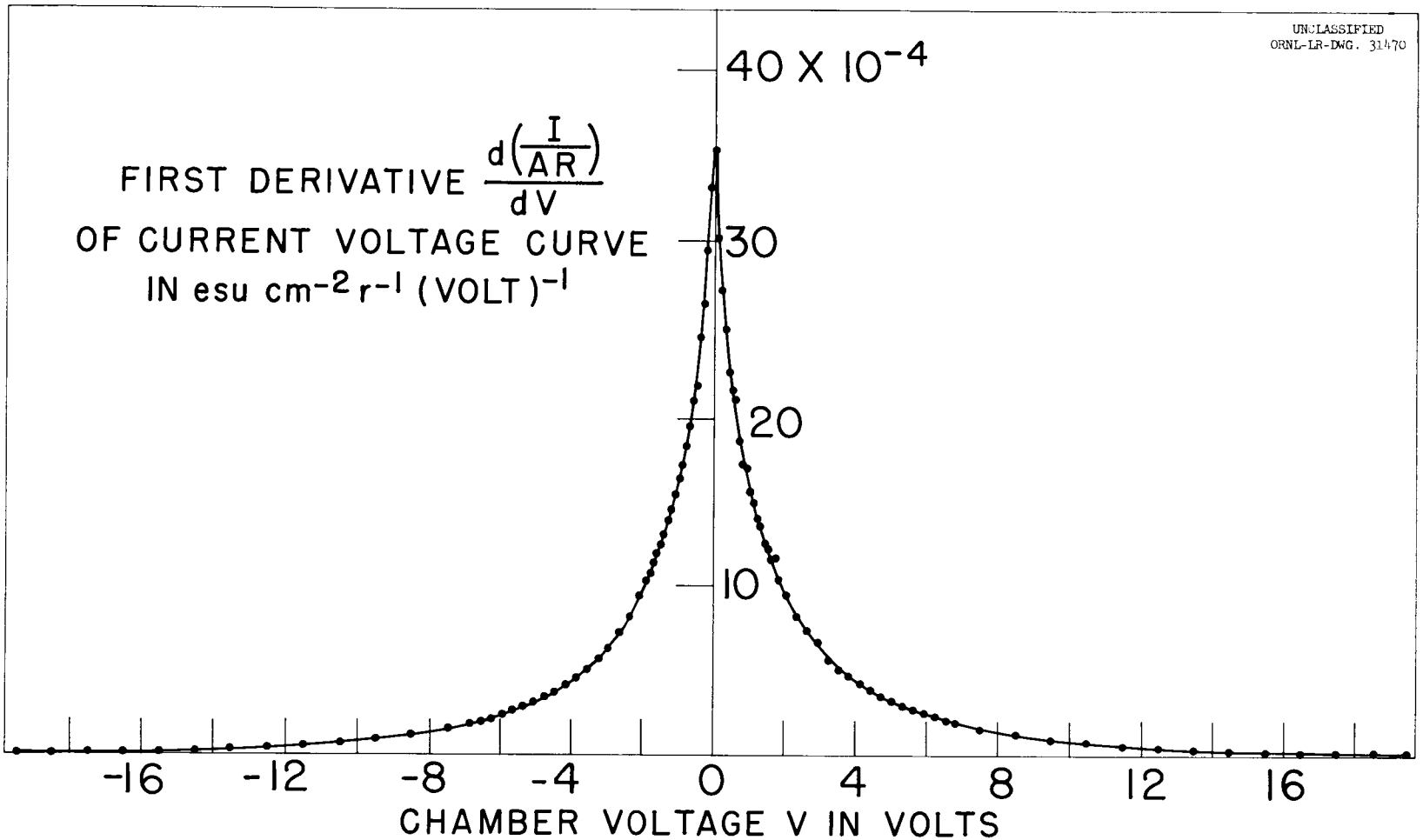

Figure 17. First Derivative of Current-Voltage Curve for Annealed Copper.

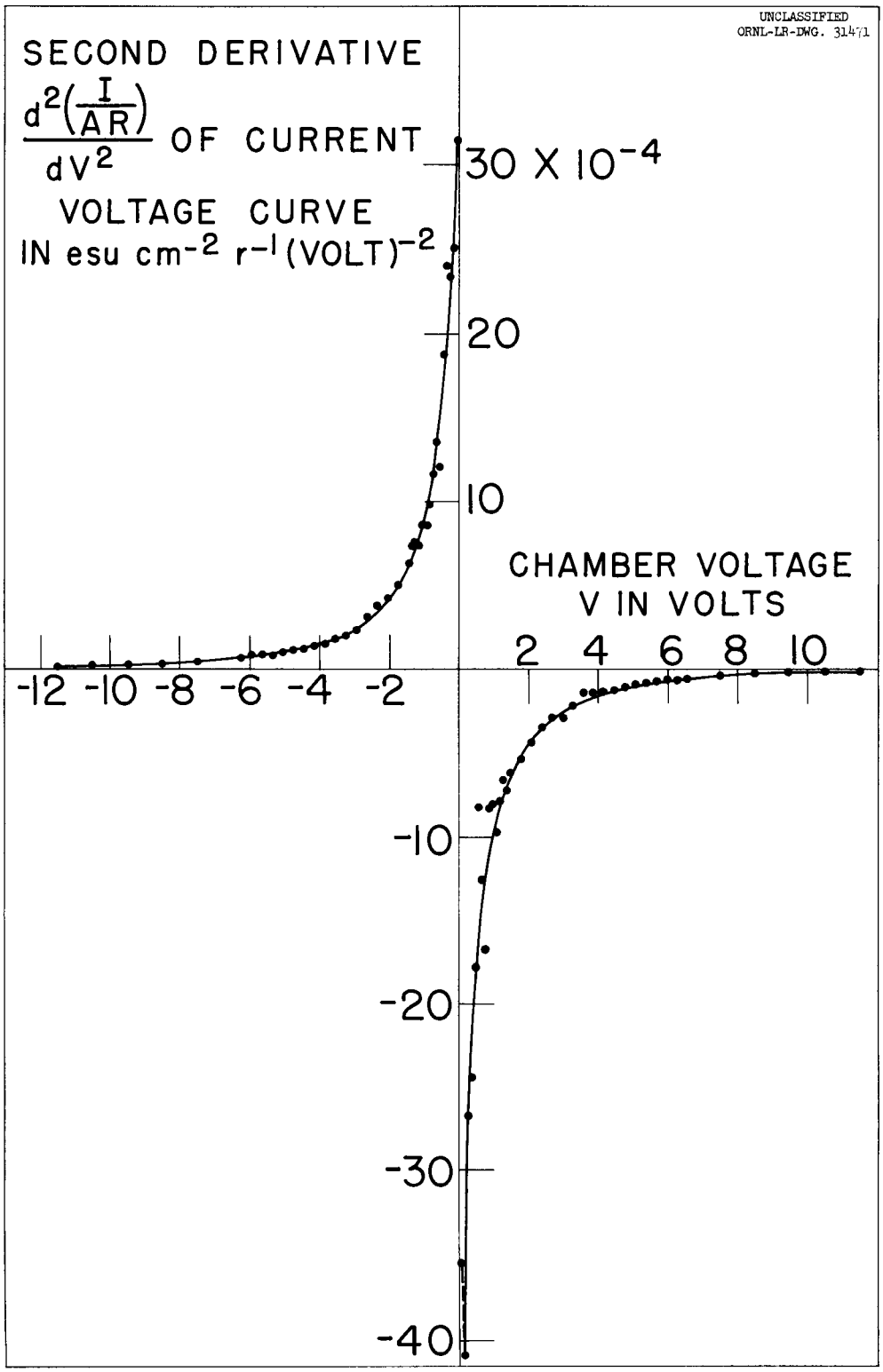

Figure 18. Second Derivative of Current-Voltage Curve for Annealed Copper.

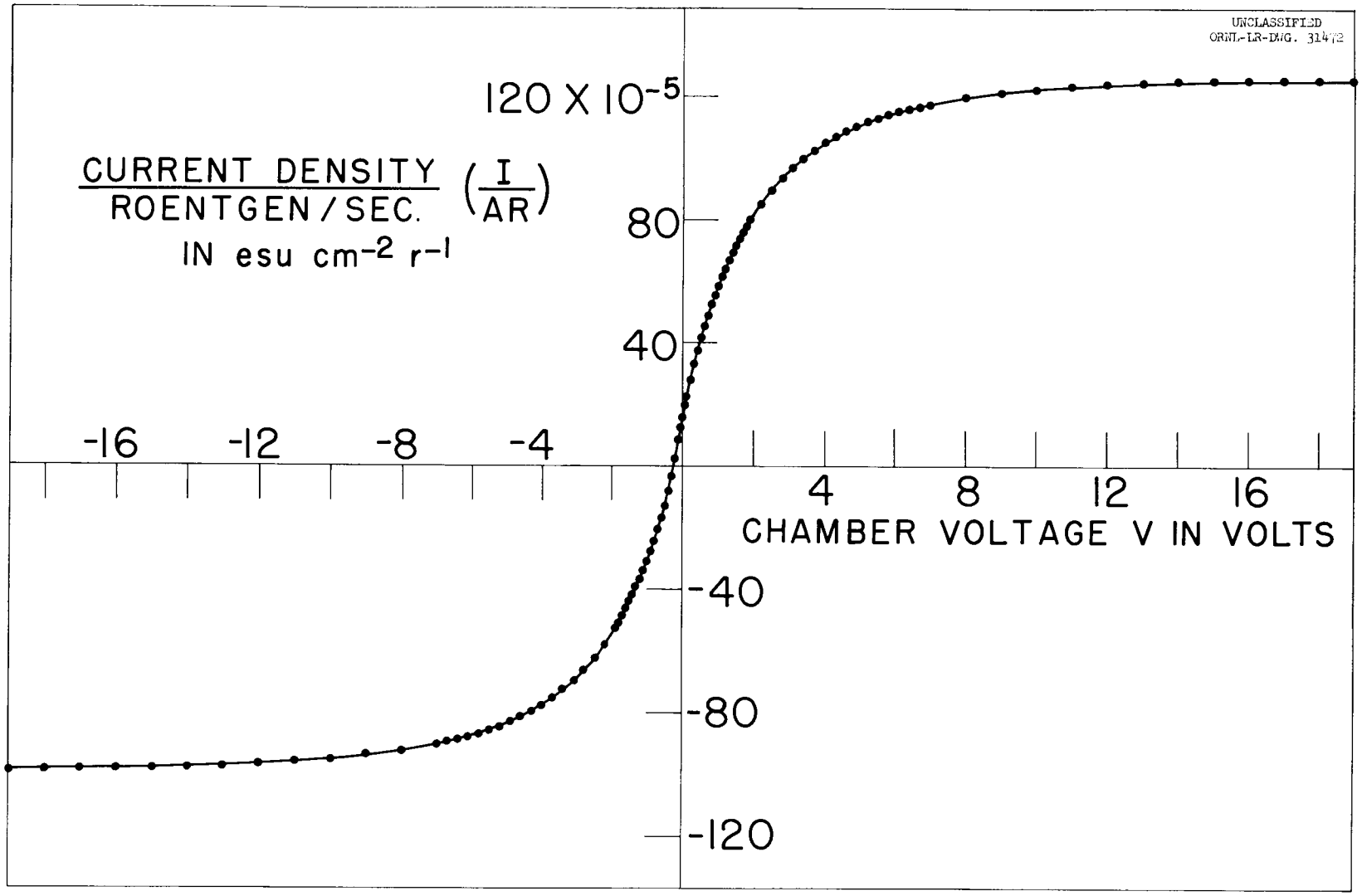

Figure 19. Current-Voltage Curve for Aluminum.

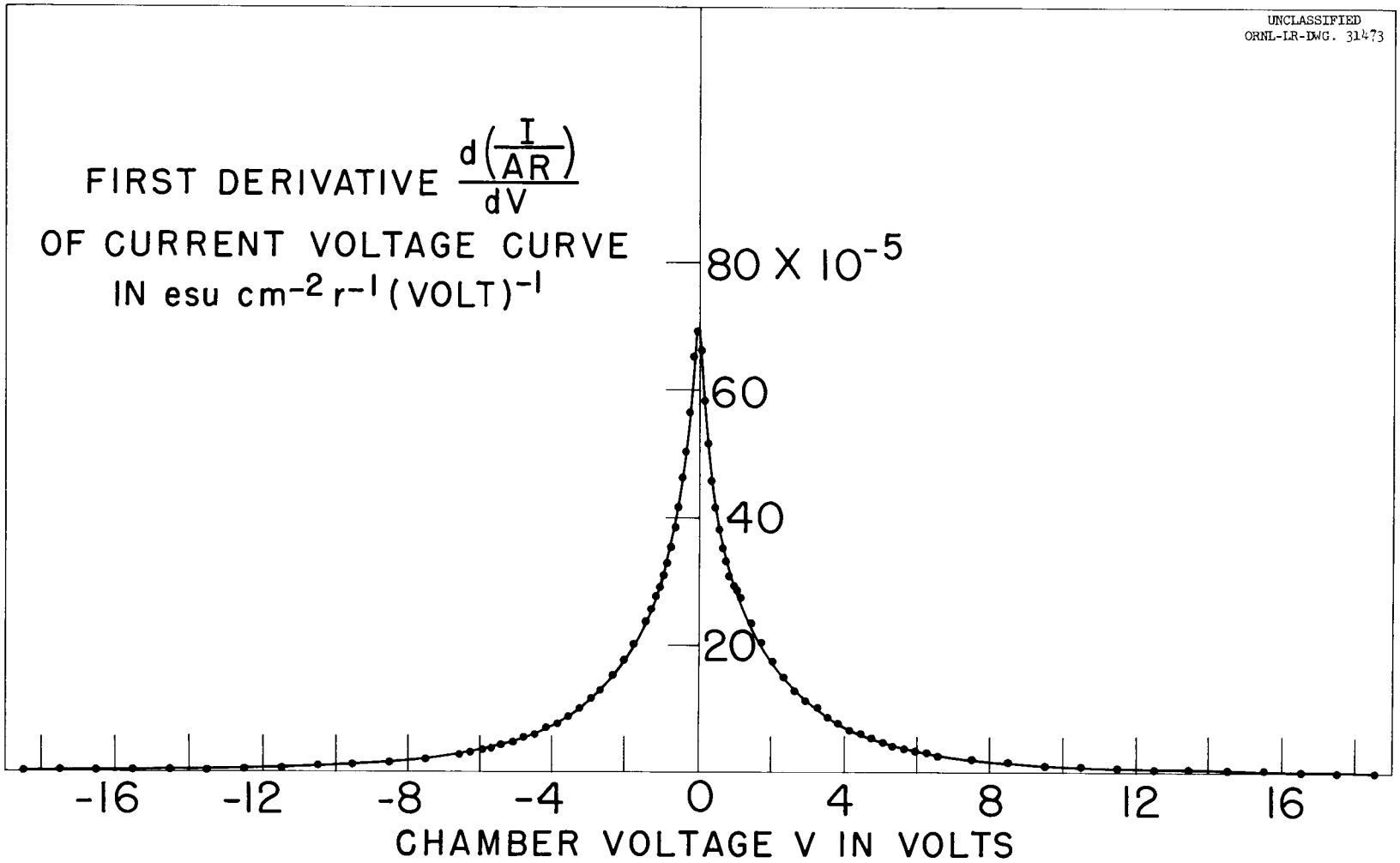

Figure 20. First Derivative of Current-Voltage Curve for Aluminum.

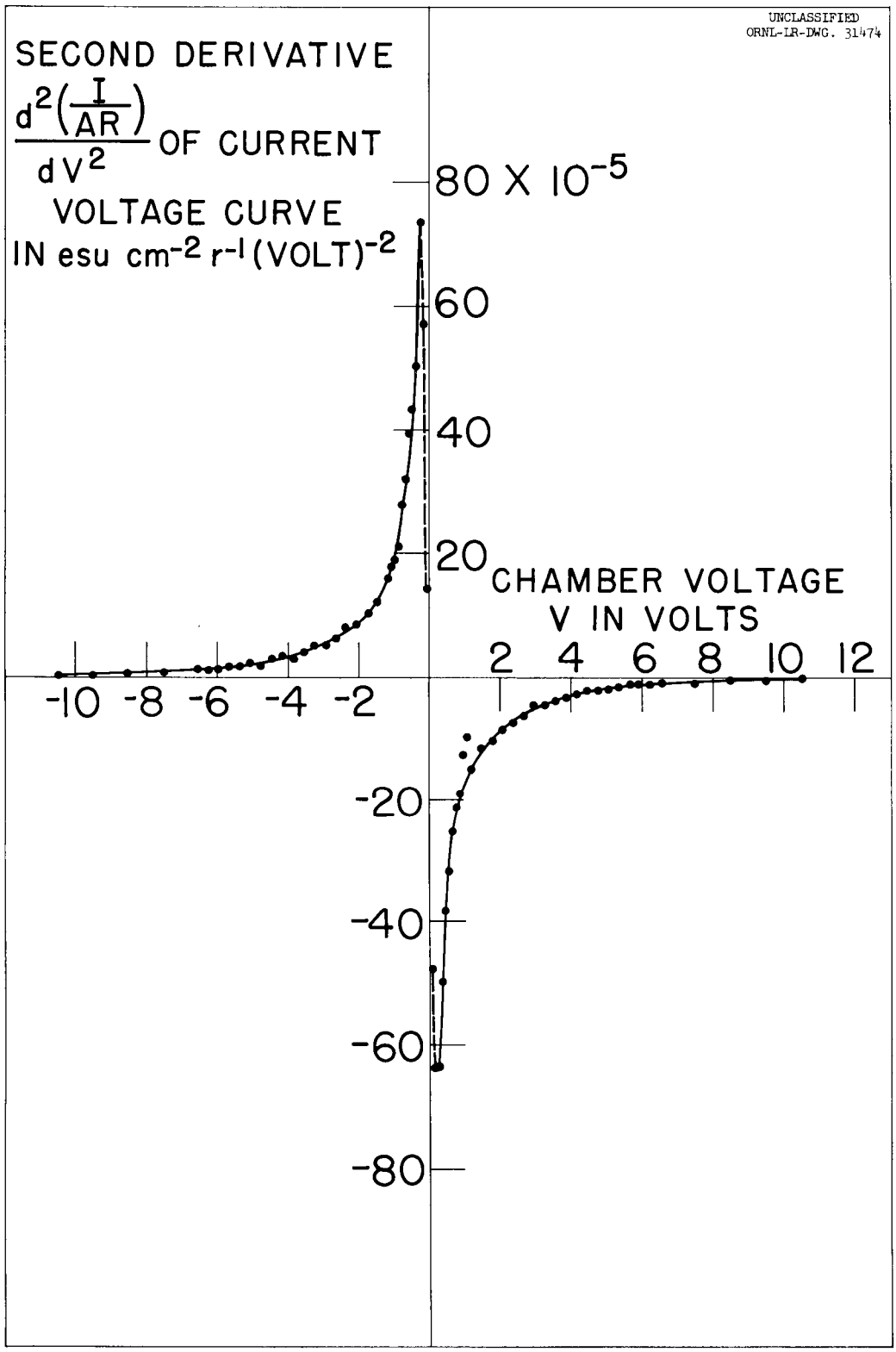

Figure 21. Second Derivative of Current-Voltage Curve for Aluminum.

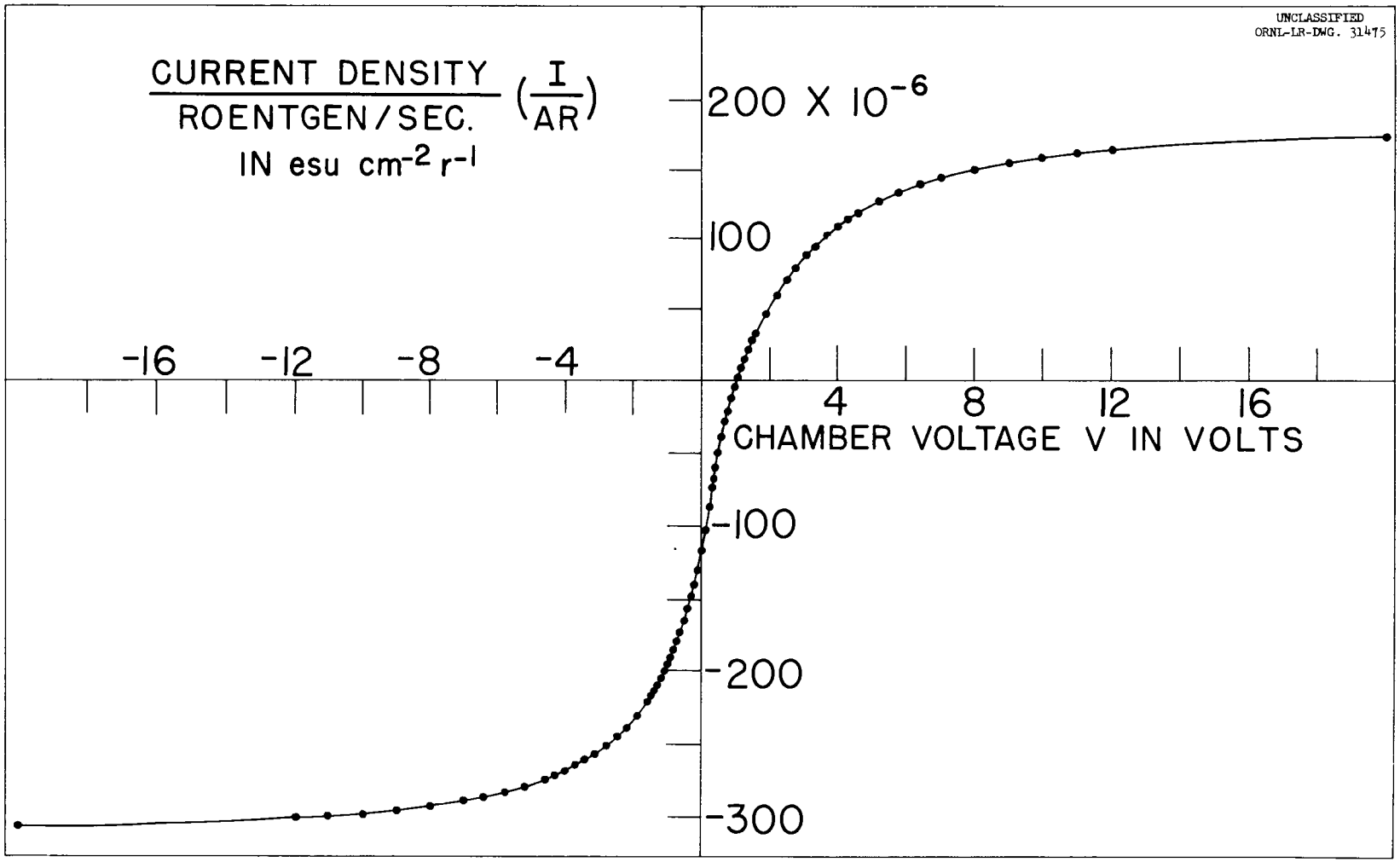

Figure 22. Current-Voltage Curve for Graphite.

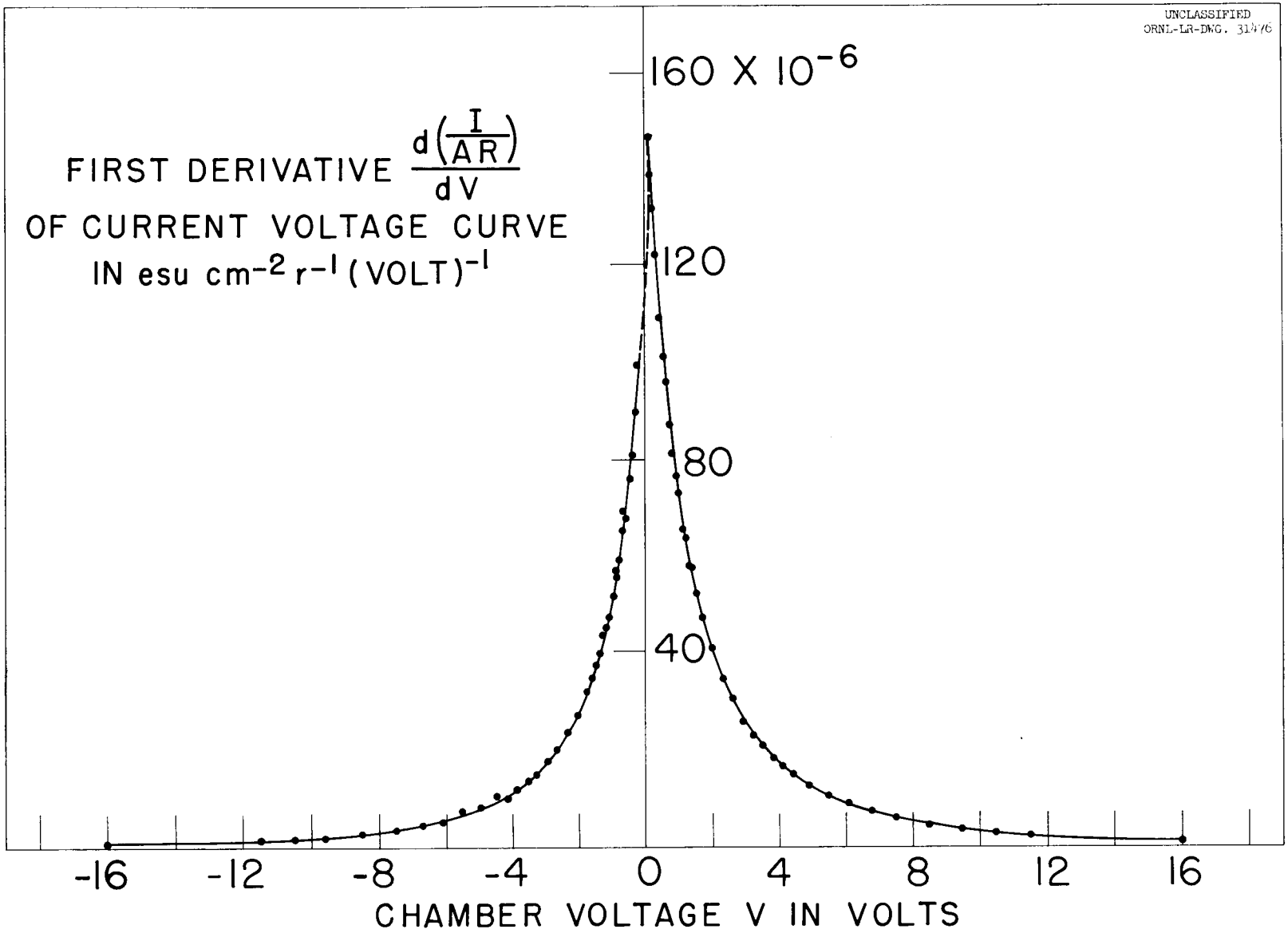

Figure 23. First Derivative of Current-Voltage Curve for Graphite.

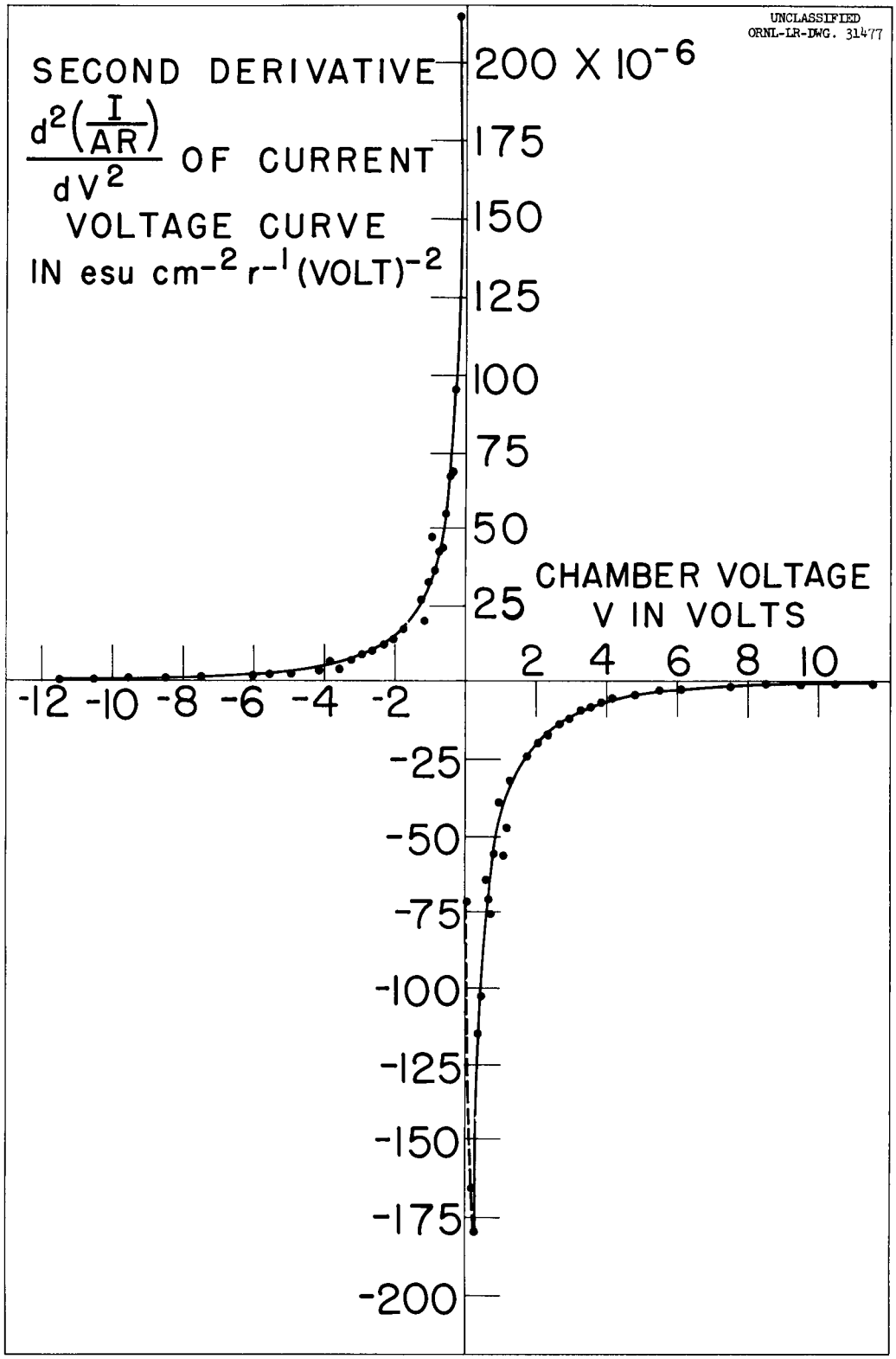

Figure 24. Second Derivative of Current-Voltage Curve for Graphite.

The calculated energy distributions for the chemically cleaned copper, annealed copper, aluminum and graphite are shown in Figures 25, 26, 27 and 28, respectively. Tables III, IV and V give the complete energy distributions for the annealed copper, aluminum and graphite, respectively.

As was expected from an earlier comparison of the chemically cleaned and annealed copper current-voltage curves, the width at half height of the energy distribution of the former exceeds that of the latter significantly. Not only were there a greater number of electrons collected from the chemically cleaned copper plates, but also the distribution was generally lower in energy than that found for annealed copper.

As was discussed in Section E of the theory, an analytic function of the form given by Equation (68) might provide a fit to the experimental energy distributions.

Figures 29, 30, 31 and 32 compare the data for the chemically cleaned copper, annealed copper, aluminum and graphite with Equation (68). The parameters α and β were adjusted by trial and error in each case to achieve the best fit.

An estimate of the accuracy of the fit was made by obtaining the saturation current density value using Equation (73) from the empirical parameters α and β. These current density values are given in Table II for comparison with the experimental values.

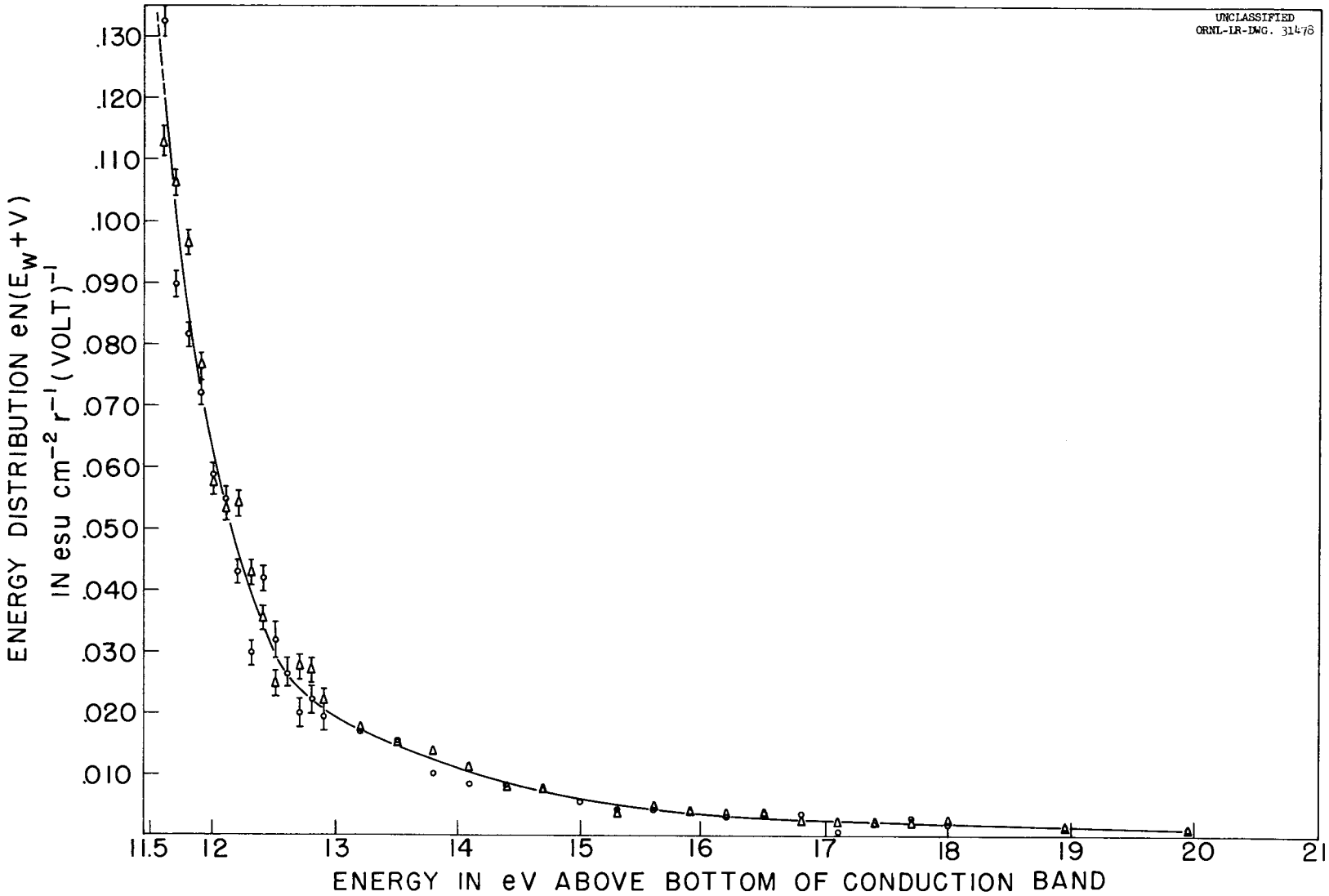

Figure 25. Energy Distribution for Chemically Cleaned Copper.

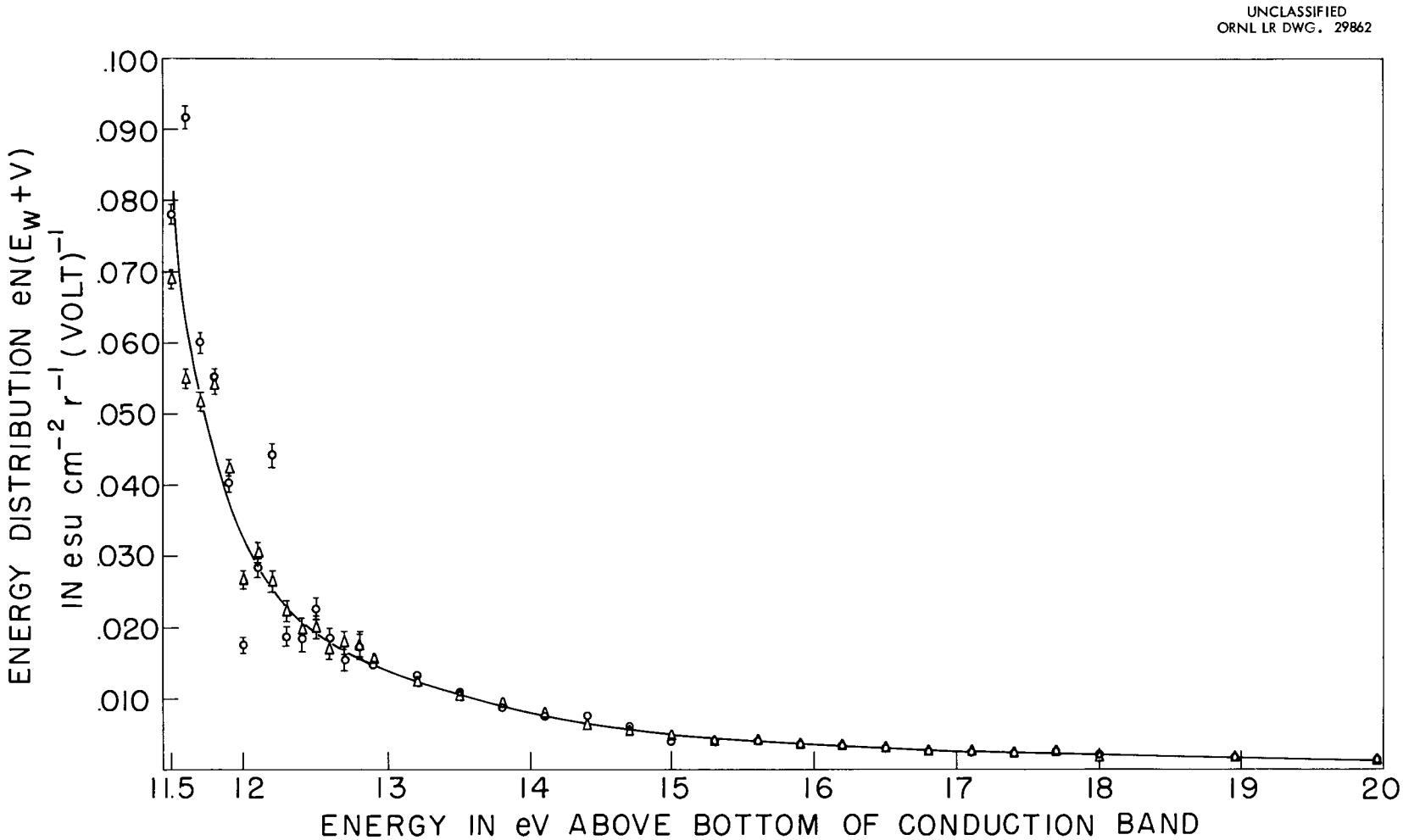

Figure 26. Energy Distribution for Annealed Copper.

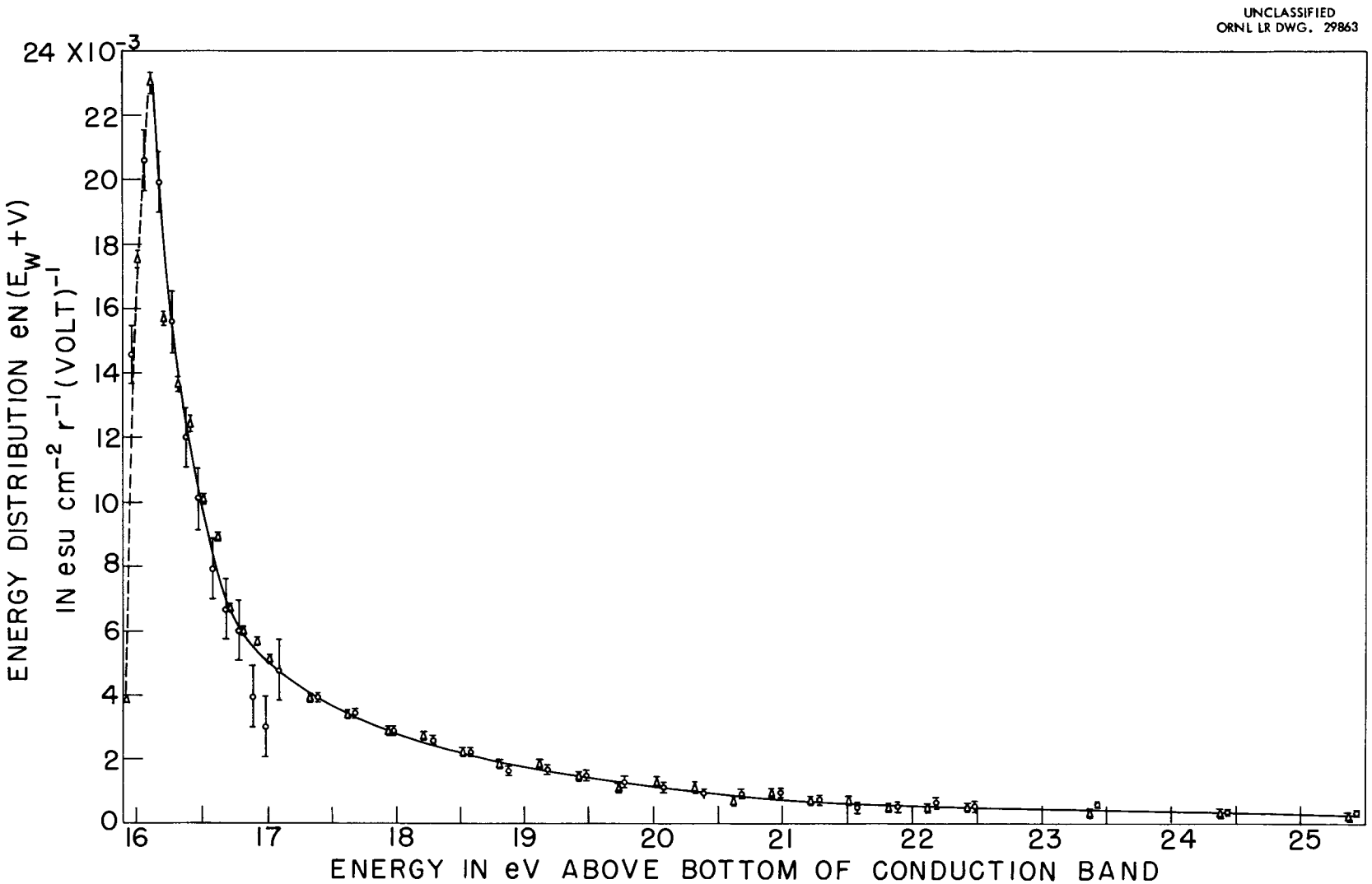

Figure 27. Energy Distribution for Aluminum.

UNCLASSIFIED
ORNL LR DWG. 29861

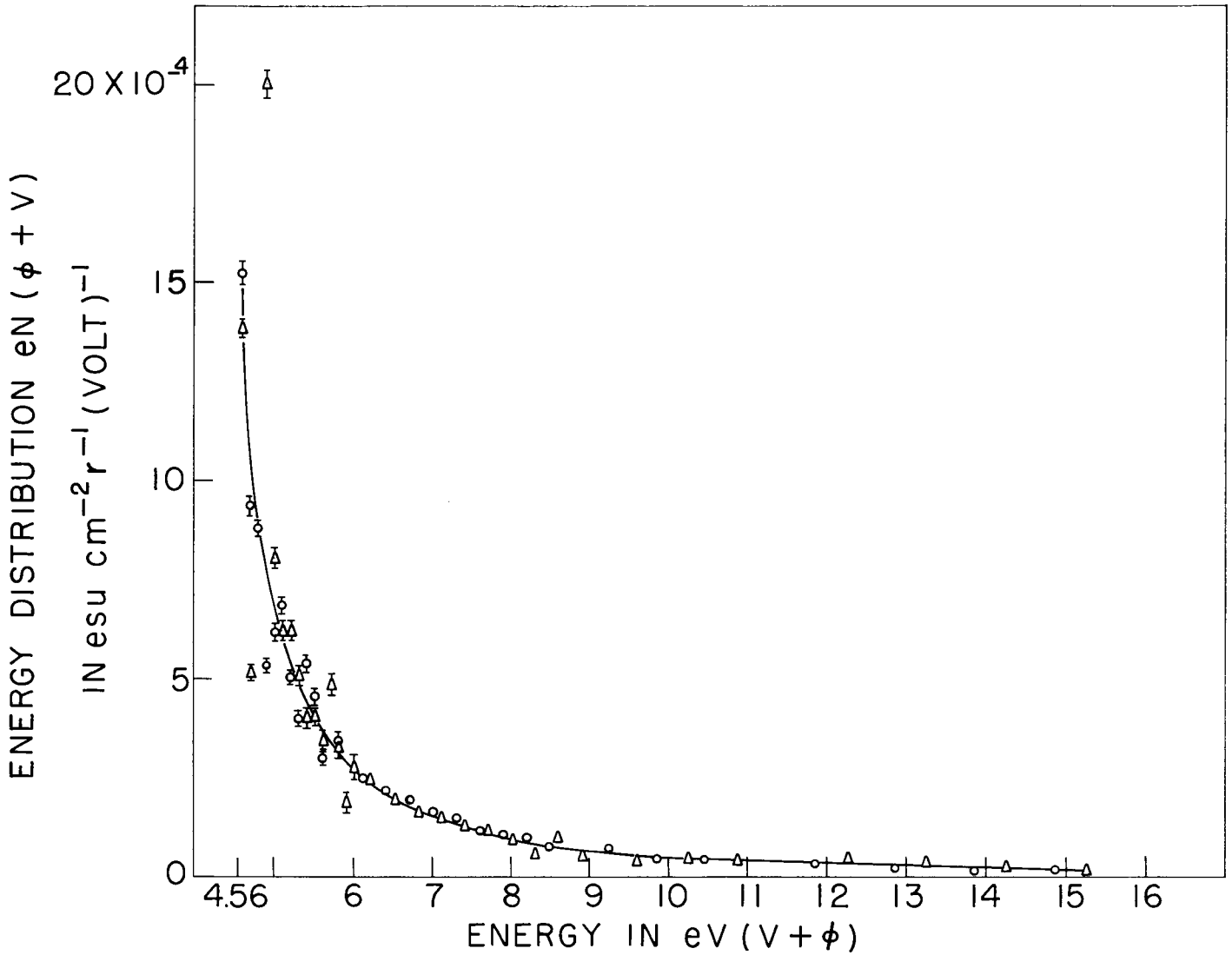

Figure 28. Energy Distribution for Graphite.

Table III. Energy Distribution in Copper (Hydrogen Annealed Surface)

V (Volts)	Upper Half Current Voltage Curve $N(E_w+V)$ $\left(\frac{esu}{cm^2 r(Volt)}\right)$	Lower Half Current Voltage Curve $N(E_w+V)$ $\left(\frac{esu}{cm^2 r(Volt)}\right)$
.05	.0780	.0689
.15	0918	.0549
.25	.0601	.0517
.35	.0552	.0541
.45	.0403	.0423
.55	.0176	.0267
.65	.0284	.0307
.75	.0442	.0265
.85	.0187	.0224
.95	.0184	.0197
1.05	.0227	.0200
1.15	.0185	.0171
1.25	.0156	.0177
1.35	.0173	.0175
1.45	.0148	.0150
1.75	.0132	.0122
2.05	.0109	.0105
2.35	.0087	.0097
2.65	.0075	.0080
2.95	.0076	.0060
3.25	.0060	.0053
3.55	.0039	.0048
3.85	.0038	.0040
4.15	.0039	.0039
4.45	.0034	.0034
4.75	.0033	.0033
5.05	.0030	.0030
5.35	.0026	.0024
5.65	.0023	.0027
5.95	.0022	.0027
6.25	.0024	.0023
6.55	.0019	.0011
7.50	.0016	.0014
8.50	.0012	.0010

Table IV. Energy Distribution in Aluminum

Upper Half Current Voltage Curve		Lower Half Current Voltage Curve	
V (Volts)	$N(E_w+V)$ $\left(\frac{esu}{cm^2 r(Volt)}\right)$	V (Volts)	$N(E_w+V)$ $\left(\frac{esu}{cm^2 r(Volt)}\right)$
.083	.0146	.017	.0038
.183	.0206	.117	.0175
.283	.0199	.217	.0230
.383	.0156	.317	.0157
.483	.0120	.417	.0136
.583	.0101	.517	.0124
.683	.0079	.617	.0101
.783	.0067	.717	.0089
.883	.0060	.817	.0067
.983	.0039	.917	.0060
1.083	.0030	1.017	.0057
1.183	.0048	1.117	.0051
1.483	.0040	1.417	.0039
1.783	.0034	1.717	.0034
2.083	.0029	2.017	.0029
2.383	.0026	2.317	.0027
2.683	.0022	2.617	.0022
2.983	.0016	2.917	.0018
3.283	.0016	3.217	.0019
3.583	.0015	3.517	.0015
3.883	.0013	3.817	.0010
4.183	.0011	4.117	.0013
4.483	.0009	4.417	.0011
4.783	.0009	4.717	.0007
5.083	.0009	5.017	.0009
5.383	.0007	5.317	.0007
5.683	.0005	5.617	.0007
5.983	.0005	5.917	.0005
6.283	.0006	6.217	.0005
6.583	.0005	6.517	.0005
7.533	.0005	7.517	.0002
8.533	.0003	8.517	.0003
9.533	.0003	9.517	.0001

Table V. Energy Distribution in Graphite

Upper Half Current Voltage Curve		Lower Half Current Voltage Curve	
V (Volts)	$N(E_w+V)$ $\left(\frac{esu}{cm^2 r(Volt)}\right)$	V (Volts)	$N(\phi+V)$ $\left(\frac{esu}{cm^2 r(Volt)}\right)$
.05	.00152	.05	.00138
.15	.00094	.15	.00051
.25	.00088		
.35	.00053	.35	.00202
.45	.00062	.45	.00080
.55	.00069	.55	.00062
.65	.00050	.65	.00062
.75	.00040	.75	.00051
.85	.00054	.85	.00040
.95	.00046	.95	.00041
1.05	.00030	1.05	.00035
1.25	.00034	1.15	.00048
1.55	.00025	1.25	.00033
1.85	.00022	1.35	.00019
2.15	.00020	1.45	.00028
2.45	.00016	1.65	.00024
2.75	.00015	1.95	.00019
3.05	.00012	2.25	.00016
3.35	.00011	2.55	.00015
3.65	.00010	2.85	.00013
3.95	.00008	3.15	.00012
4.70	.00007	3.45	.00010
5.30	.00005	3.75	.00006
5.90	.00004	4.05	.00010
7.30	.00003	4.35	.00005
8.30	.00002	5.10	.00004
9.30	.00002	5.70	.00004
10.30	.00002	6.30	.00004
		7.70	.00005
		8.70	.00004
		9.70	.00003
		10.70	.00002

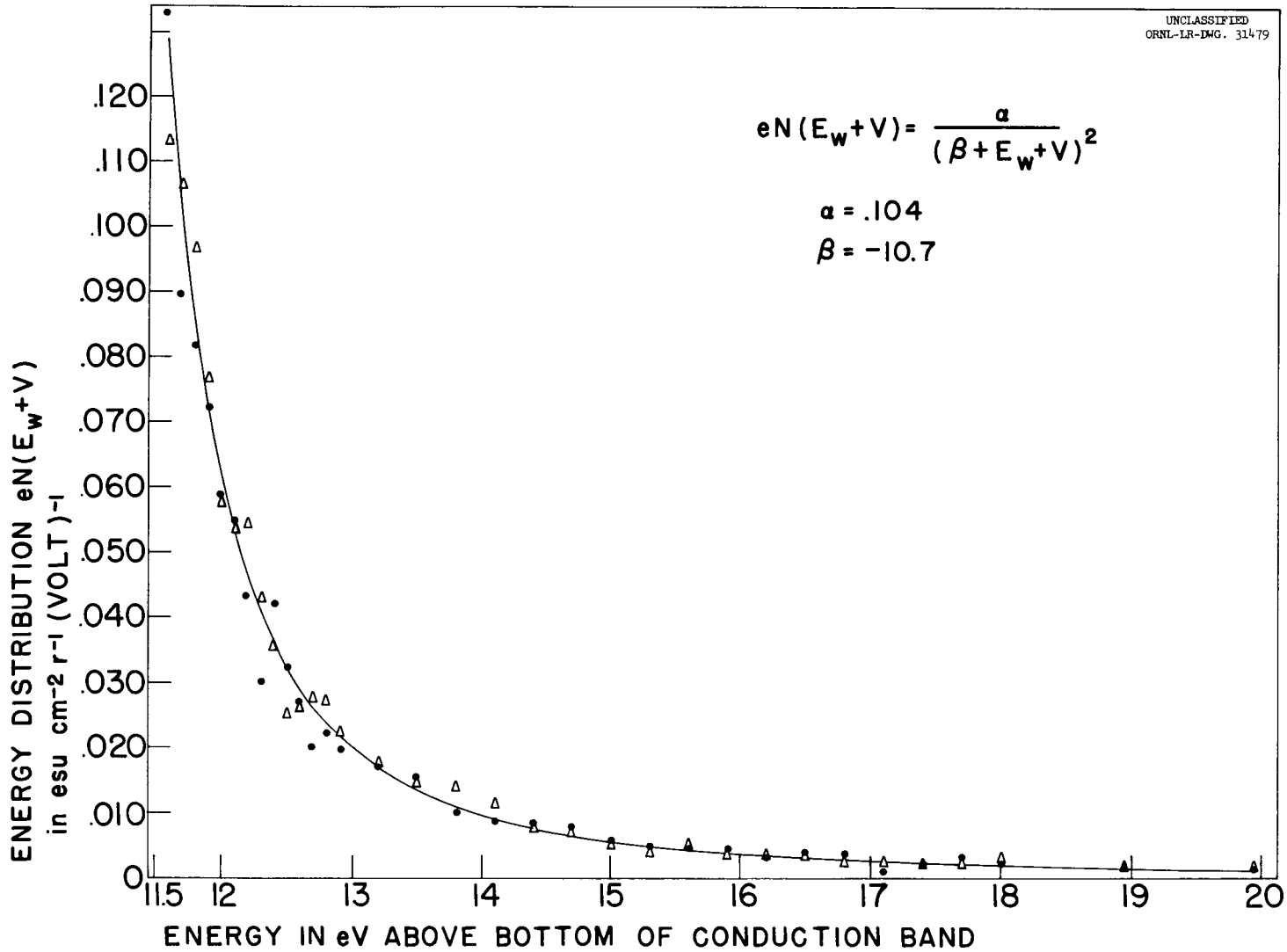

Figure 29. The Fit of the Function $\alpha/(\beta+E_W+V)^2$ to the Energy Distribution for Chemically Cleaned Copper.

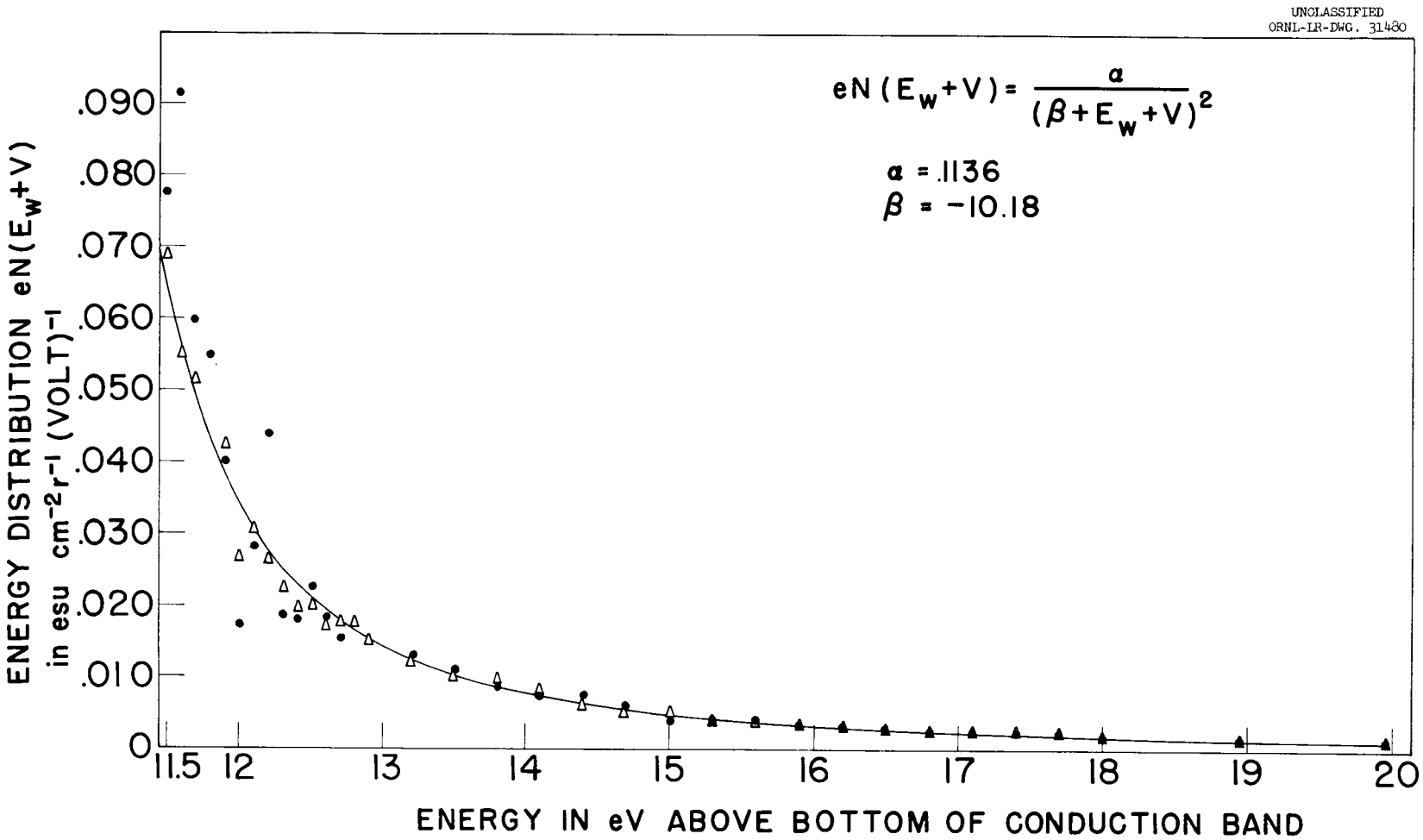

Figure 30. The Fit of the Function $\alpha/(\beta+E_W+V)^2$ to the Energy Distribution for Annealed Copper.

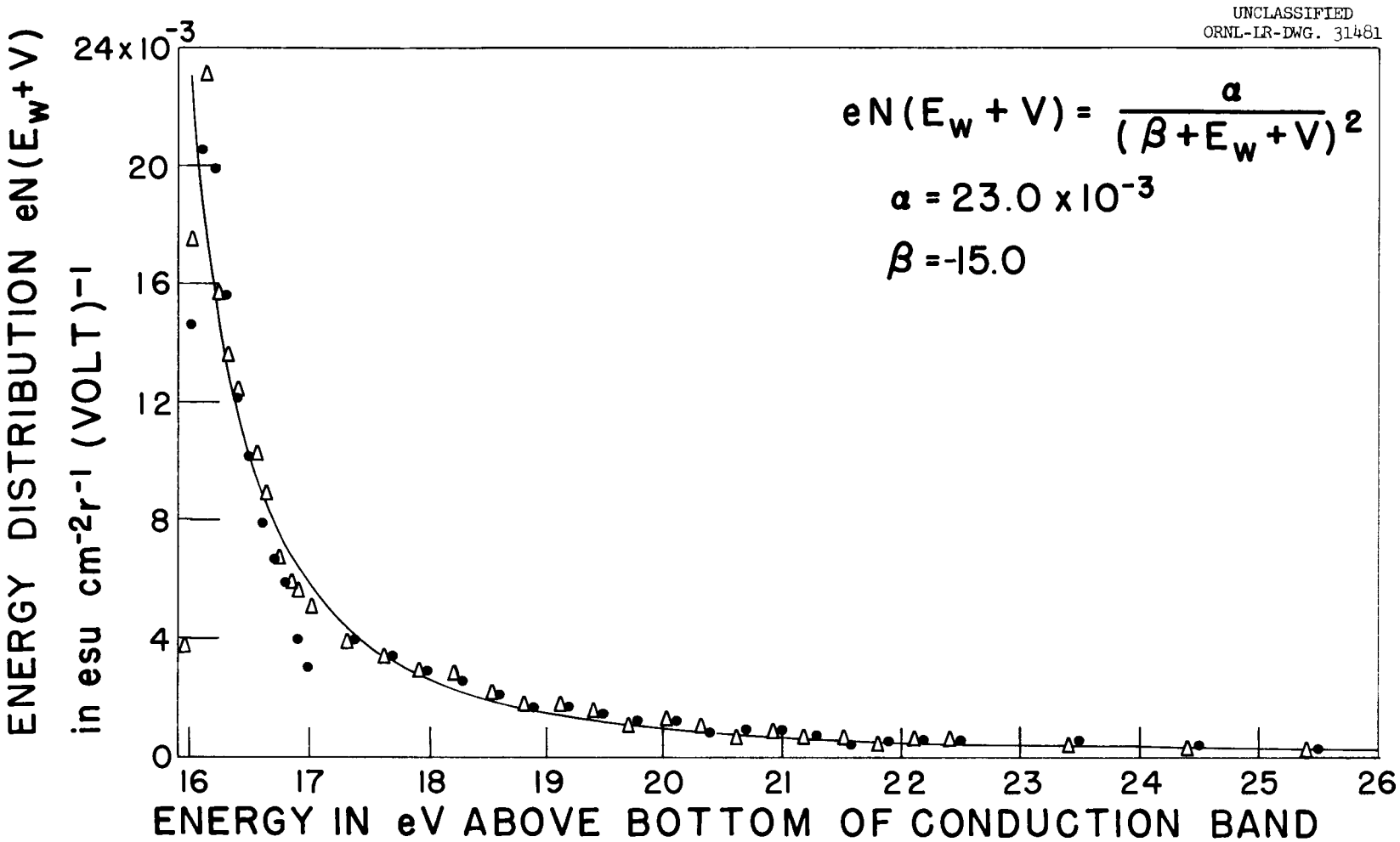

Figure 31. The Fit of the Function $\alpha/(\beta+E_W+V)^2$ to the Energy Distribution for Aluminum.

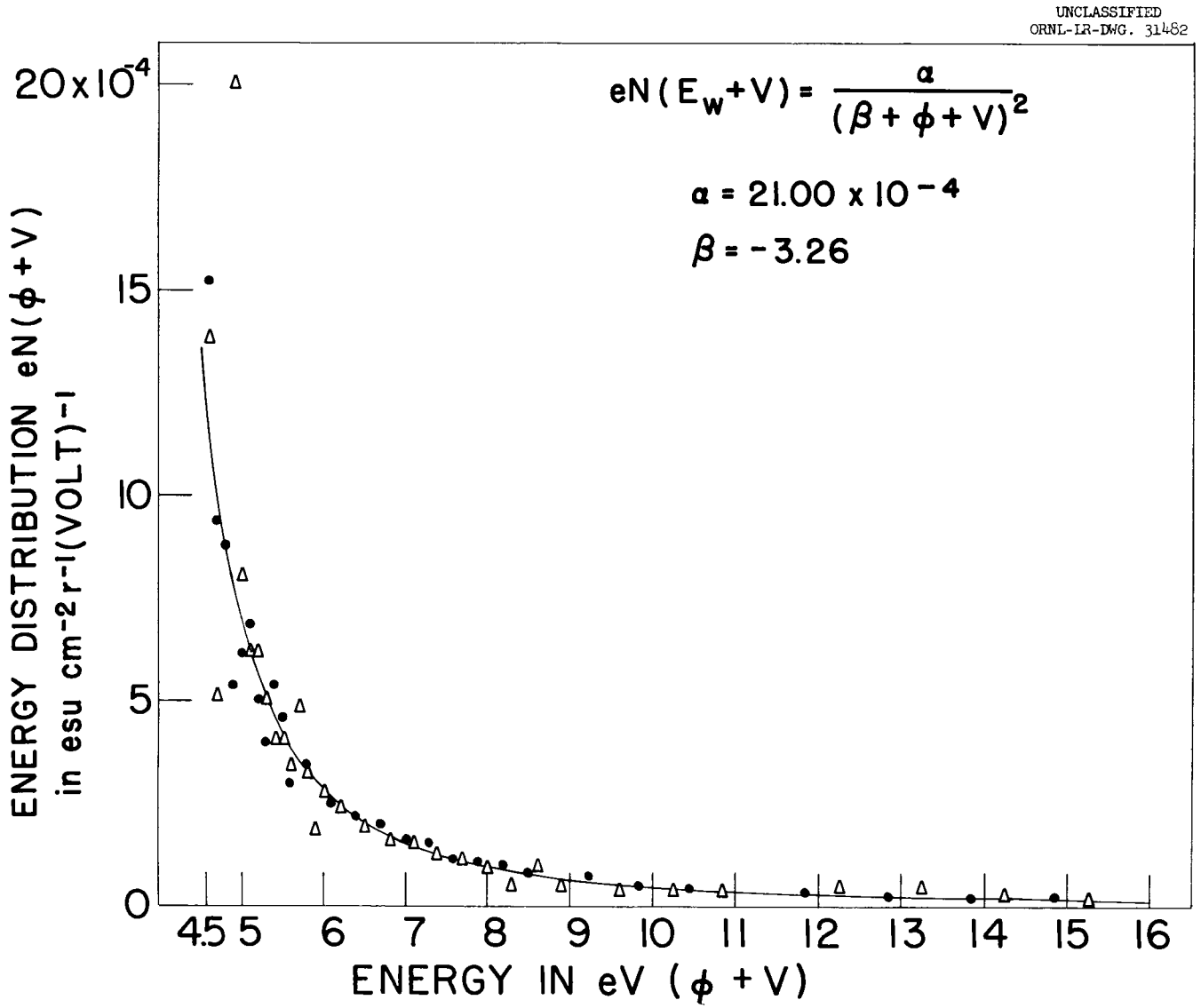

Figure 32. The Fit of the Function $\alpha/(\beta+\phi+V)^2$ to the Energy Distribution of Graphite.

VI. CONCLUSIONS

Parallel plate chambers constructed of copper, aluminum and graphite were bombarded with lightly filtered X-rays generated by a 250 KVCP machine. From the current-voltage curves of these chambers at effectively zero gas pressure, the energy distributions of the electrons inside the media were found. These energy distributions were found to depend on the first and second derivatives of the current-voltage curve. The distributions all showed a relatively large number of low energy electrons, having a width at half height of about $E_W + 0.5$ and approaching zero at about $E_W + 20$ where E_W is the sum of the Fermi energy and the photoelectric work function.

A comparison of the experimental current-voltage curves with those obtained from Greening's energy distribution indicates that the energy distributions of this work have a much larger number of low energy electrons than the distribution proposed by Greening.

Surface conditions were found to influence the current-voltage curves and energy distributions. In the case of copper a layer of copper oxide on the plate surface increased the relative number of low energy electrons in the energy distributions and increased also the chamber saturation current density. This is in accordance with the usual behavior of oxide coatings which tend to reduce the photoelectric work function, thereby allowing lower energy electrons to escape from the surface.

All energy distributions could be fitted well with an analytic function of the form $\frac{\alpha}{(\beta+E_w+V)^2}$. Saturation currents based on the empirical constants α and β were found to check the observed saturation current closely.

In all cases the value of β was found to be about equal to $(1-E_w)$. Thus all distributions could be represented by the function

$$\frac{\alpha}{\left[E-(E_w-1) \right]^2}$$

where E is the electron energy and α varies from one material to another.

APPENDIX I

Sample Energy Distribution Calculation

A portion of the experimental data and analysis for annealed copper is given in Table VI. A step-by-step sample calculation of each operation performed in the analysis is given below.

As indicated in Table VI, the first operation is the calculation of the output voltage ratio V_R/V_{RM}.

For the values given for a chamber voltage V of .7 volts, the ratio becomes

$$\frac{V_R}{V_{RM}} = \frac{2.2549 \text{ volts}}{5.4374 \text{ volts}} = .414702 \quad . \tag{a}$$

The current ratio, (I/I_M) is obtained by dividing each of the voltages V_R and V_{RM} by their respective electrometer resistors R and R_M giving

$$\frac{I}{I_M} = \frac{V_R/R}{V_{RM}/R_M} = \frac{V_R}{V_{RM}} \times \frac{R_M}{R} \quad . \tag{b}$$

For the voltage ratio for a chamber voltage V of .7 volts the current ratio becomes

$$\frac{I}{I_M} = .414702 \times \frac{.973 \times 10^{10} \text{ ohms}}{.960 \times 10^{10} \text{ ohms}} = .42032 \quad . \tag{c}$$

Table VI. Sample of Data and Analysis for Annealed Copper (Lower Plates Positive)

V	V_R	V_{RM}	V_R/V_{RM}	$I/I_M = \frac{V_R}{V_{RM}} \times \frac{R_M}{R}$	$I/AR = I/I_M \times (\overline{I_M/AR})$	$\frac{d(I/AR)}{dV}$	$\frac{d^2(I/AR)}{dV^2}$	$2(E_w+V)$	$-2(E_w+V) \times \frac{d^2(I/AR)}{dV^2}$	$eN(E_w+V)$
.5 .55	1.7380	5.4388	.319556	.32388	.0013441	.002077				
.6 .65	2.0065	5.4388	.368923	.37392	.0015518	.001925	-.00135	24.2	.03267	.0307
.7 .75	2.2549	5.4374	.414702	.42032	.0017443	.001807	-.00116	24.4	.02830	.0265
.8 .85	2.4885	5.4374	.457664	.46386	.0019250	.001694	-.00098	24.6	.02411	.0224
.9 .95	2.7075	5.4375	.497931	.50467	.0020944	.001612				
1.0	2.9158	5.4373	.536259	.54352	.0022556					

In order to express the currents, the first and second derivatives and the energy distribution in appropriate units, (I/I_M) can be multiplied by the average value $(\overline{I_M/AR})$ giving

$$\frac{I}{I_M} \times (\overline{I_M/AR}) = \frac{I}{AR} \quad . \tag{d}$$

The average V_{RM} value of 5.46 volts from Table VI, and the values of A and R_M given in the supplement to Table VI along with the ratio (I/I_M) calculated in (c) yield

$$\frac{I}{AR} = .42032\ (I_M/AR) = .42032\ \frac{V_{RM}/R_M}{AR}$$

$$= .42032 \times \frac{5.46 \text{ volts}/.973 \times 10^{10} \text{ ohms}}{147.63 \text{ cm}^2 \times 2.75 \text{ roentgen/sec}} \times 3 \times 10^9 \text{ esu/coul} \tag{e}$$

or

$$\frac{I}{AR} = .42032 \times .00415\ \frac{\text{esu}}{\text{cm}^2\text{r}} = .0017443\ \frac{\text{esu}}{\text{cm}^2\text{r}} \quad .$$

The I/AR values given in Table VI obtained at chamber voltages of .6 and .7 volts are used to obtain the first derivative at .65 volts.

$$\frac{d(I/AR)}{dV} = \frac{y_{i+1} - y_i}{\Delta x} = \frac{.0017443 - .0015518}{.1} \tag{f}$$

or

$$= .001925\ \frac{\text{esu}}{\text{cm}^2\text{r(volt)}} \quad .$$

The second derivative also at .65 volts is calculated using the (I/AR) values given in Table VI for chamber voltages of .5, .6, .7 and .8 volts.

$$\frac{d^2(I/AR)}{dV^2} = \frac{y_{i+3}-y_{i+2}-y_{i+1}+y_i}{2\,\Delta\,x^2} = \frac{.0019250-.0017443-.0015518+.0013441}{2(.1)^2}$$

or

$$\frac{d^2(I/AR)}{dV^2} \equiv .00135 \quad \frac{esu}{cm^2 r(volt)^2} \quad . \qquad (g)$$

In order to obtain the energy distribution it is necessary to multiply the second derivative by $-2(E_w+V)$ and then subtract the first derivative from this value. For copper, E_w which is the sum of the Fermi energy E_F = 7.0 volts and the photoelectric work function ϕ = 4.45 volts is equal to 11.45 volts as given in Table VII.

The value of the energy distribution $eN(E_w+V)$ at the applied chamber voltage of .65 volts is then

$$eN(E_w+V) = -2(E_w+V)\ \frac{d^2(I/AR)}{dV^2} - \frac{d(I/AR)}{dV}$$

$$= (-24.2)(-.00135) - .001925 \qquad (h)$$

$$eN(E_w+V) = .0307 \quad \frac{esu}{cm^2 r(volt)} \quad .$$

Throughout the data analysis more than the correct number of significant figures have been carried for reasons of internal consistency. The final energy distributions have been rounded off to the correct number of significant figures.

Table VII. Fermi Energy E_F and Photoelectric Work Function Φ for Cu, Al and Graphite.

	E_F(eV)	Φ(eV)
Copper[14]	7.00	4.45
Aluminum[14]	11.7	4.20
Graphite[15]	~ 0	4.56

[14] Dekker, A. J., SOLID STATE PHYSICS, (Prentice Hall, New York, 1957) p. 215.

[15] Taft, E., and Opker, L., Phys. Rev. 99, 1831 (1955).

TABLE VI SUPPLEMENT

Explanation of Symbols and Values of Constants Used in Table VI

V = Test chamber collecting voltage in volts.

V_M = Monitor chamber collecting voltage in volts.

I = Test chamber current in amperes at chamber voltage V.

I_M = Monitor chamber current in amperes at chamber voltage V_M.

R = $.960 \times 10^{10}$ ohms = electrometer resistor carrying test chamber current I.

R_M = $.973 \times 10^{10}$ ohms = electrometer resistor carrying monitor chamber current I_M.

V_R = $I\ R$ = test chamber output voltage in volts.

V_{RM} = $I\ R_M$ = 5.46 volts = average value of monitor chamber output voltage for dose rate of 2.75 roentgens/sec.

A = 147.63 cm^2 = average irradiated test chamber plate area.

R = 2.75 roentgens/sec = average dose rate between test chamber plates measured in air with Victoreen chamber.

E_w = 11.45 volts.

R_M/R = 1.0135

$(\overline{I_M/AR})$ = $.00415\ \frac{esu}{cm^2 r}$.

APPENDIX II

A. Error Analysis

Error estimates for the final energy distributions were obtained by considering only the deviations in the second derivatives. That is, not only was the first derivative term in Equation (67) smaller than the second derivative term usually by at least one order of magnitude, but the per cent error in the first derivative was smaller that the per cent error in the second derivative as well.

Let

$$D_1 = \pm \frac{2\sqrt{(\Delta V_{i+1})^2 + (\Delta V_i)^2}}{(V_{i+1} - V_i)^2} , \qquad (a)$$

where D_1 is the per cent deviation of the denominator of the second derivative (Equation 76), and ΔV_i is the deviation in the applied chamber voltage V_i.

Let

$$D_2 = \pm \frac{\sqrt{(\Delta y_{i+3})^2 + (\Delta y_{i+2})^2 + (\Delta y_{i+1})^2 + (\Delta y_i)^2}}{(y_{i+3} - y_{i+2} - y_{i+1} + y_i)} , \qquad (b)$$

where D_2 is the per cent deviation of the numerator of the second derivative (Equation 76) and Δy_i is the deviation of the current

value, $(I/AR)_i$. Therefore, D the total deviation in per cent of the second derivative is given by

$$D = \pm \sqrt{D_1^2 + D_2^2} \quad . \qquad (c)$$

B. Sample Error Calculation for Annealed Copper

In Table VIII there is tabulated a portion of the annealed copper data with the corresponding error analysis. The deviations of $\pm$ 0.00005, $\pm$ 0.0005, and $\pm$ 0.0012 assigned to V, V_R and V_{RM} respectively were determined in the following manner. The deviation of $\pm$ 0.00005 volts for the test plate collecting voltage V was the smallest voltage change which could easily be detected with a Rubicon (Pot. 2) High Precision Type B potentiometer using a 0.004 μa/mm Leeds Northrup Galvanometer. The deviations of $\pm$ 0.0005 volts and $\pm$ 0.0012 volts given for the output voltages V_R and V_{RM} corresponded to the smallest bucking voltage change which could be detected on the 10 mv recorders of the respective chambers. The test chamber electrometer had a full scale deflection sensitivity of 0.15 volts as compared to 0.29 volts for the monitor chamber electrometer which accounts for the difference in the V_R and V_{RM} deviations.

Table VIII. Error Analysis for Annealed Copper

V	V_R	V_{RM}	$\Delta V_R(\%)$	$\Delta V_{RM}(\%)$	$\frac{\Delta y_i}{y_i}(\%)$	y_i	Δy_i	D_1	$(y_{i+3}-y_{i+2}-y_{i+1}+y_i)$	See Below	D_2	D	$\frac{DeN(E_w+V)}{cm^2 r}$ esu
.50000 ±.00005	1.7380 ±.0005	5.4388 ±.0012	.0287	.0221	.0362	1344.1 $\times 10^{-6}$	.486 $\times 10^{-6}$	1.41%					
.60000 ±.00005	2.0065 ±.0005	5.4388 ±.0012	.0249	.0221	.0336	1551.8 $\times 10^{-6}$	.521 $\times 10^{-6}$	1.41%	27.0 $\times 10^{-6}$	1.065 $\times 10^{-6}$	3.95%	4.43%	$\pm 1.36 \times 10^{-3}$
.70000 ±.00005	2.2549 ±.0005	5.4374 ±.0012	.0222	.0221	.0313	1744.3 $\times 10^{-6}$	.546 $\times 10^{-6}$	1.41%	23.2 $\times 10^{-6}$	1.123 $\times 10^{-6}$	4.85%	5.05%	$\pm 1.34 \times 10^{-3}$
.80000 ±.00005	2.4885 ±.0005	5.4374 ±.0012	.0201	.0221	.0298	1925.0 $\times 10^{-6}$	.574 $\times 10^{-6}$	1.41%	19.6 $\times 10^{-6}$	1.183 $\times 10^{-6}$	6.04%	6.21%	$\pm 1.39 \times 10^{-3}$
.90000 ±.00005	2.7075 ±.0005	5.4375 ±.0012	.0185	.0221	.0288	2094.4 $\times 10^{-6}$	.604 $\times 10^{-6}$	1.41%					
1.00000 ±.00005	2.9158 ±.0005	5.4373 ±.0012	.0171	.0221	.0279	2255.6 $\times 10^{-6}$	.630 $\times 10^{-6}$						

Caption for Column 11: $\sqrt{(\Delta y_{i+3})^2+(\Delta y_{i+2})^2+(\Delta y_{i+1})^2+\Delta y_i^2}$

After calculating the percent voltage deviations, $\Delta V_R(\%)$ and $\Delta V_{RM}(\%)$ of the test and monitor chambers the per cent deviation in the current $(I/AR)_i$ was found by taking the square root of the sum of the squares of these quantities. Therefore

$$\frac{\Delta y_i}{y_i}(\%) = \pm \left[\Delta V_R(\%) \right]^2 + \left[\Delta V_{RM}(\%) \right]^2 . \qquad \text{(d)}$$

For example, for a test plate collecting voltage V of .6 volts, this is

$$\frac{\Delta y_i}{y_i}(\%) = \pm \sqrt{(.0249)^2 + (.0221)^2} = \pm .0336\% . \qquad \text{(e)}$$

Now the absolute deviation Δy_i of the current value for the collecting voltage V of .6 volts is

$$y_i \times \frac{\Delta y_i}{y_i} = \pm .000336 \times .0015518 = \pm .521 \times 10^{-6} \ \frac{\text{esu}}{\text{cm}^2\text{r}} , \qquad \text{(f)}$$

where $y_i = (I/AR)_i = .0015518$ esu/cm^{2}r.

The per cent deviation D_1 of the denominator of the expression for the second derivative is given by (a). If one substitutes for

the voltage deviation $\Delta V_i = \pm 0.00005$, and for the voltage mesh $(V_{i+1}-V_i) = 0.1$ volt,

$$D_1 = \frac{2\sqrt{(.00005)^2 + (.00005)^2}}{(.1)^2} = \frac{14.14 \times 10^{-5}}{.01} = \pm 1.41\% \quad . \tag{g}$$

The per cent deviation D_2 of the second derivative numerator is given by (b). When substitution is made for the current values y_i and deviations Δy_i for the collecting voltages V of .5, .6, .7 and .8 volts (b) gives

$$D_2 = \frac{10^{-6}\sqrt{(.574)^2 + (.546)^2 + (.521)^2 + (.486)^2}}{10^{-6}(1925.0 - 1744.3 - 1551.8 + 1344.1)} = \frac{1.065 \times 10^{-6}}{27.0 \times 10^{-6}} \tag{h}$$

or

$$D_2 = \pm 3.95\% \quad .$$

The per cent deviation D in the second derivative according to Equation (c) becomes

$$D = \pm \sqrt{(1.41\%)^2 + (3.95\%)^2} = \pm 4.43\% \quad . \tag{i}$$

The absolute value of the error is obtained by multiplying the value .0307 esu from Table VI for a chamber voltage V of .65 volts by D the total deviation error in the energy distribution

$$D \times eN(E_w+V) = \pm 4.43\% \times .0307 = \pm .00136 \frac{esu}{cm^2 r} .$$

The other energy distribution deviations have been calculated similarily. These deviations are indicated on the energy distributions shown in Figures 25, 26, 27 and 28.

APPENDIX III

SUMMARY OF ABBREVIATIONS AND SYMBOLS

A = Average irradiated test chamber plate area.

e = Electronic charge.

E_F = Fermi energy.

E_i = Energy of electrons inside the medium.

E_o = V - energy of electrons outside medium.

ϕ = Photoelectric work function.

E_w = $E_F + \phi$ - minimum energy an electron must have in order to escape from the medium.

V = Test chamber collecting voltage.

V_M = Monitor chamber collecting voltage.

V_R = Test chamber output voltage.

V_{RM} = Monitor chamber output voltage.

I = Test chamber current.

I_M = Monitor chamber current.

R = Test chamber electrometer resistance.

R_M = Monitor chamber electrometer resistance.

R = Dose rate in roentgens/sec between test chamber plates.

r = Dose in roentgens.

Bibliography

Birkhoff, R. D., Hubbell, H. H. Jr., Cheka, J. S., and Ritchie, R. H., "Spectral Distribution of Electron Flux in a Beta-Radioactive Medium", Health Physics, 1, 27 (1958).

Dekker, A. J., SOLID STATE PHYSICS, (Prentice Hall, New York, 1957).

Greening, J. R., "A Contribution to the Theory of Ionization Chamber Measurements at Low Pressures", Brit. J. of Rad., 27, No. 315, 163 (1954).

McKay, K. G., "Secondary Electron Emission", Advances in Electronics, 1, (Academic Press, Inc., New York, 1948).

Platzman, R. L., "Subexcitation Electrons", Rad. Res., 2, 1 (1955).

Spencer, L. V., and Fano, U., "Energy Spectrum Resulting from Electrons Slowing Down", Phys. Rev. 93, 1172 (1954).

Taft, E., and Opker, L., "Photoelectric Emission from Polycrystalling Graphite", Phys. Rev. 99, 1831 (1955).

Taylor, L. S., "The Measurement of X- and Gamma Radiation Over a Wide Energy Range", Brit. J. of Rad., 24, No. 278, 67 (1951).

Wolff, P. A., "Theory of Secondary Electron Cascade in Metals", Phys. Rev., 95, No. 1, 56 (1954).

ORNL-2521
Physics and Mathematics
TID-4500 (13th ed., Rev.)
February 15, 1958

INTERNAL DISTRIBUTION

1. C. E. Center
2. Biology Library
3. Health Physics Library
4-5. Central Research Library
6. Reactor Experimental Engineering Library
7-26. Laboratory Records Department
27. Laboratory Records, ORNL R.C.
28. L. B. Emlet (K-25)
29. J. P. Murray (Y-12)
30. A. M. Weinberg
31. J. A. Swartout
32. E. D. Shipley
33. M. L. Nelson
34. K. Z. Morgan
35. S. C. Lind
36. A. S. Householder
37. C. S. Harrill
38. C. E. Winters
39. A. H. Snell
40. E. H. Taylor
41. W. H. Jordan
42. T. A. Lincoln
43. A. Hollaender
44. F. L. Culler
45. H. E. Seagren
46. D. Phillips
47. M. T. Kelley
48. E. E. Anderson
49. R. S. Livingston
50. C. P. Keim
51. K. E. Cowser
52. C. D. Susano
53. L. B. Farabee
54. F. J. Davis
55. R. J. Morton
56. C. E. Haynes
57. E. G. Struxness
58. W. E. Cohn
59-109. H. H. Hubbell, Jr.
110. D. E. Arthur
111. J. Neufeld
112. M. J. Skinner
113. J. C. Hart
114. T. H. J. Burnett
115. W. J. Lacy
116. G. S. Hurst
117. T. E. Bortner
118. J. A. Lane
119. H. P. Yockey
120. C. E. Clifford
121. J. L. Gabbard
122. R. A. Charpie
123. D. M. Davis
124. P. E. Brown
125. E. D. Gupton
126. J. C. Ledbetter
127. R. L. Clark
128. G. C. Cain
129. L. C. Johnson
130. W. W. Ogg
131. O. D. Teague
132. E. L. Sharp
133. E. J. Kuna
134. H. H. Abee
135. C. R. Guinn
136. A. D. Warden
137. C. C. Sartain
138. J. R. Muir
139. J. A. Auxier
140. M. F. Fair
141. S. I. Auerbach
142. G. W. Royster, Jr.
143. R. R. Dickison
144. F. W. Sanders
145. F. C. Maienschein
146. W. J. Boegly, Jr.
147. F. L. Parker
148. W. E. Lotz
149. B. Fish
150. M. B. Edwards
151. F. M. Empson
152. G. G. Robeck
153-202. R. D. Birkhoff
203. R. H. Ritchie
204. J. A. Harter
205. R. M. Johnson
206. W. G. Stone
207. J. S. Cheka
208. P. N. Hensley
209. R. W. Peelle
210-230. D. R. Nelson
231. E. B. Wagner
232. C. A. Preskitt

233. S. K. Allison (consultant)
234. W. H. Langham (consultant)
235. A. Wolman (consultant)
236. R. Zirkle (consultant)
237. L. S. Taylor (consultant)
238. ORNL - Y-12 Technical Library, Document Reference Section

EXTERNAL DISTRIBUTION

239. Knolls Atomic Power Laboratory, Schenectady (Robert J. Feinberg, GE employee)
240. 1st Lt. John C. Villforth, 58 Diana Lane, West, Fairbarn, Ohio
241. Willard O. Olson, 328 Liberty St., Mankato, Minn.
242. Industrial Reactor Laboratories, Inc., Plainsboro, N.J. (Andrew P. Hull)
243. Jay S. Mendell, 700 West 175th St., New York, N.Y.
244. Physics Department, Purdue University, Lafayette, Ind. (R. L. Platzman)
245-773. Given distribution as shown in TID-4500 (13th ed., Rev.) under Physics and Mathematics category
774. Division of Research and Development, AEC, ORO